



# CHORUS

This is the accepted manuscript made available via CHORUS. The article has been published as:

## Amplitude analysis of the $\pi^0\pi^0$ system produced in radiative $J/\psi$ decays

M. Ablikim *et al.* (BESIII Collaboration)

Phys. Rev. D **92**, 052003 — Published 14 September 2015

DOI: [10.1103/PhysRevD.92.052003](https://doi.org/10.1103/PhysRevD.92.052003)

# An amplitude analysis of the $\pi^0\pi^0$ system produced in radiative $J/\psi$ decays

M. Ablikim<sup>1</sup>, M. N. Achasov<sup>9,f</sup>, X. C. Ai<sup>1</sup>, O. Albayrak<sup>5</sup>, M. Albrecht<sup>4</sup>, D. J. Ambrose<sup>44</sup>, A. Amoroso<sup>48A,48C</sup>, F. F. An<sup>1</sup>,  
Q. An<sup>45,a</sup>, J. Z. Bai<sup>1</sup>, R. Baldini Ferrolli<sup>20A</sup>, Y. Ban<sup>31</sup>, D. W. Bennett<sup>19</sup>, J. V. Bennett<sup>5</sup>, M. Bertani<sup>20A</sup>, D. Bettini<sup>21A</sup>,  
J. M. Bian<sup>43</sup>, F. Bianchi<sup>48A,48C</sup>, E. Boger<sup>23,d</sup>, O. Bondarenko<sup>25</sup>, I. Boyko<sup>23</sup>, R. A. Briere<sup>5</sup>, H. Cai<sup>50</sup>, X. Cai<sup>1,a</sup>, O. Cakir<sup>40A,b</sup>,  
A. Calcaterra<sup>20A</sup>, G. F. Cao<sup>1</sup>, S. A. Cetin<sup>40B</sup>, J. F. Chang<sup>1,a</sup>, G. Chelkov<sup>23,d,e</sup>, G. Chen<sup>1</sup>, H. S. Chen<sup>1</sup>, H. Y. Chen<sup>2</sup>,  
J. C. Chen<sup>1</sup>, M. L. Chen<sup>1,a</sup>, S. J. Chen<sup>29</sup>, X. Chen<sup>1,a</sup>, X. R. Chen<sup>26</sup>, Y. B. Chen<sup>1,a</sup>, H. P. Cheng<sup>17</sup>, X. K. Chu<sup>31</sup>,  
G. Cibinetto<sup>21A</sup>, D. Cronin-Hennessy<sup>43</sup>, H. L. Dai<sup>1,a</sup>, J. P. Dai<sup>34</sup>, A. Dbeyssi<sup>14</sup>, D. Dedovich<sup>23</sup>, Z. Y. Deng<sup>1</sup>, A. Denig<sup>22</sup>,  
I. Denysenko<sup>23</sup>, M. Destefanis<sup>48A,48C</sup>, F. De Mori<sup>48A,48C</sup>, Y. Ding<sup>27</sup>, C. Dong<sup>30</sup>, J. Dong<sup>1,a</sup>, L. Y. Dong<sup>1</sup>, M. Y. Dong<sup>1,a</sup>,  
S. X. Du<sup>52</sup>, P. F. Duan<sup>1</sup>, E. E. Eren<sup>40B</sup>, J. Z. Fan<sup>39</sup>, J. F. Fang<sup>1,a</sup>, S. S. Fang<sup>1</sup>, X. Fang<sup>45,a</sup>, Y. Fang<sup>1</sup>, L. Fava<sup>48B,48C</sup>,  
F. Feldbauer<sup>22</sup>, G. Felici<sup>20A</sup>, C. Q. Feng<sup>45,a</sup>, E. Fioravanti<sup>21A</sup>, M. Fritsch<sup>14,22</sup>, C. D. Fu<sup>1</sup>, Q. Gao<sup>1</sup>, X. Y. Gao<sup>2</sup>, Y. Gao<sup>39</sup>,  
Z. Gao<sup>45,a</sup>, I. Garzia<sup>21A</sup>, C. Geng<sup>45,a</sup>, K. Goetzen<sup>10</sup>, W. X. Gong<sup>1,a</sup>, W. Gradl<sup>22</sup>, M. Greco<sup>48A,48C</sup>, M. H. Gu<sup>1,a</sup>, Y. T. Gu<sup>12</sup>,  
Y. H. Guan<sup>1</sup>, A. Q. Guo<sup>1</sup>, L. B. Guo<sup>28</sup>, Y. Guo<sup>1</sup>, Y. P. Guo<sup>22</sup>, Z. Haddadi<sup>25</sup>, A. Hafner<sup>22</sup>, S. Han<sup>50</sup>, Y. L. Han<sup>1</sup>, X. Q. Hao<sup>15</sup>,  
F. A. Harris<sup>42</sup>, K. L. He<sup>1</sup>, Z. Y. He<sup>30</sup>, T. Held<sup>4</sup>, Y. K. Heng<sup>1,a</sup>, Z. L. Hou<sup>1</sup>, C. Hu<sup>28</sup>, H. M. Hu<sup>1</sup>, J. F. Hu<sup>48A,48C</sup>, T. Hu<sup>1,a</sup>,  
Y. Hu<sup>1</sup>, G. M. Huang<sup>6</sup>, G. S. Huang<sup>45,a</sup>, H. P. Huang<sup>50</sup>, J. S. Huang<sup>15</sup>, X. T. Huang<sup>33</sup>, Y. Huang<sup>29</sup>, T. Hussain<sup>47</sup>, Q. Ji<sup>1</sup>,  
Q. P. Ji<sup>30</sup>, X. B. Ji<sup>1</sup>, X. L. Ji<sup>1,a</sup>, L. L. Jiang<sup>1</sup>, L. W. Jiang<sup>50</sup>, X. S. Jiang<sup>1,a</sup>, X. Y. Jiang<sup>30</sup>, J. B. Jiao<sup>33</sup>, Z. Jiao<sup>17</sup>,  
D. P. Jin<sup>1,a</sup>, S. Jin<sup>1</sup>, T. Johansson<sup>49</sup>, A. Julin<sup>43</sup>, N. Kalantar-Nayestanaki<sup>25</sup>, X. L. Kang<sup>1</sup>, X. S. Kang<sup>30</sup>, M. Kavatsyuk<sup>25</sup>,  
B. C. Ke<sup>5</sup>, P. Kiese<sup>22</sup>, R. Kliemt<sup>14</sup>, B. Kloss<sup>22</sup>, O. B. Kolcu<sup>40B,i</sup>, B. Kopf<sup>4</sup>, M. Kornicer<sup>42</sup>, W. Kuhn<sup>24</sup>, A. Kupsc<sup>49</sup>,  
J. S. Lange<sup>24</sup>, M. Lara<sup>19</sup>, P. Larin<sup>14</sup>, C. Leng<sup>48C</sup>, C. Li<sup>49</sup>, C. H. Li<sup>1</sup>, Cheng Li<sup>45,a</sup>, D. M. Li<sup>52</sup>, F. Li<sup>1,a</sup>, G. Li<sup>1</sup>, H. B. Li<sup>1</sup>,  
J. C. Li<sup>1</sup>, Jin Li<sup>32</sup>, K. Li<sup>13</sup>, K. Li<sup>33</sup>, Lei Li<sup>3</sup>, P. R. Li<sup>41</sup>, T. Li<sup>33</sup>, W. D. Li<sup>1</sup>, W. G. Li<sup>1</sup>, X. L. Li<sup>33</sup>, X. M. Li<sup>12</sup>, X. N. Li<sup>1,a</sup>,  
X. Q. Li<sup>30</sup>, Z. B. Li<sup>38</sup>, H. Liang<sup>45,a</sup>, Y. F. Liang<sup>36</sup>, Y. T. Liang<sup>24</sup>, G. R. Liao<sup>11</sup>, D. X. Lin<sup>14</sup>, B. J. Liu<sup>1</sup>, C. X. Liu<sup>1</sup>,  
F. H. Liu<sup>35</sup>, Fang Liu<sup>1</sup>, Feng Liu<sup>6</sup>, H. B. Liu<sup>12</sup>, H. H. Liu<sup>16</sup>, H. H. Liu<sup>1</sup>, H. M. Liu<sup>1</sup>, J. Liu<sup>1</sup>, J. B. Liu<sup>45,a</sup>, J. P. Liu<sup>50</sup>,  
J. Y. Liu<sup>1</sup>, K. Liu<sup>39</sup>, K. Y. Liu<sup>27</sup>, L. D. Liu<sup>31</sup>, P. L. Liu<sup>1,a</sup>, Q. Liu<sup>41</sup>, S. B. Liu<sup>45,a</sup>, X. Liu<sup>26</sup>, X. X. Liu<sup>41</sup>, Y. B. Liu<sup>30</sup>,  
Z. A. Liu<sup>1,a</sup>, Zhiqiang Liu<sup>1</sup>, Zhiqing Liu<sup>22</sup>, H. Loehner<sup>25</sup>, X. C. Lou<sup>1,a,h</sup>, H. J. Lu<sup>17</sup>, J. G. Lu<sup>1,a</sup>, R. Q. Lu<sup>18</sup>, Y. Lu<sup>1</sup>,  
Y. P. Lu<sup>1,a</sup>, C. L. Luo<sup>28</sup>, M. X. Luo<sup>51</sup>, T. Luo<sup>42</sup>, X. L. Luo<sup>1,a</sup>, M. Lv<sup>1</sup>, X. R. Lyu<sup>41</sup>, F. C. Ma<sup>27</sup>, H. L. Ma<sup>1</sup>, L. L. Ma<sup>33</sup>,  
Q. M. Ma<sup>1</sup>, T. Ma<sup>1</sup>, X. N. Ma<sup>30</sup>, X. Y. Ma<sup>1,a</sup>, F. E. Maas<sup>14</sup>, M. Maggiora<sup>48A,48C</sup>, Q. A. Malik<sup>47</sup>, Y. J. Mao<sup>31</sup>, Z. P. Mao<sup>1</sup>,  
S. Marcello<sup>48A,48C</sup>, J. G. Messchendorp<sup>25</sup>, J. Min<sup>1,a</sup>, T. J. Min<sup>1</sup>, R. E. Mitchell<sup>19</sup>, X. H. Mo<sup>1,a</sup>, Y. J. Mo<sup>6</sup>, C. Morales  
Morales<sup>14</sup>, K. Moriya<sup>19</sup>, N. Yu. Muchnoi<sup>9,f</sup>, H. Muramatsu<sup>43</sup>, Y. Nefedov<sup>23</sup>, F. Nerling<sup>14</sup>, I. B. Nikolaev<sup>9,f</sup>, Z. Ning<sup>1,a</sup>,  
S. Nisar<sup>8</sup>, S. L. Niu<sup>1,a</sup>, X. Y. Niu<sup>1</sup>, S. L. Olsen<sup>32</sup>, Q. Ouyang<sup>1,a</sup>, S. Pacetti<sup>20B</sup>, P. Patteri<sup>20A</sup>, M. Pelizaeus<sup>4</sup>, H. P. Peng<sup>45,a</sup>,  
K. Peters<sup>10</sup>, J. Pettersson<sup>49</sup>, J. L. Ping<sup>28</sup>, R. G. Ping<sup>1</sup>, R. Poling<sup>43</sup>, V. Prasad<sup>1</sup>, Y. N. Pu<sup>18</sup>, M. Qi<sup>29</sup>, S. Qian<sup>1,a</sup>, C. F. Qiao<sup>41</sup>,  
L. Q. Qin<sup>33</sup>, N. Qin<sup>50</sup>, X. S. Qin<sup>1</sup>, Y. Qin<sup>31</sup>, Z. H. Qin<sup>1,a</sup>, J. F. Qiu<sup>1</sup>, K. H. Rashid<sup>47</sup>, C. F. Redmer<sup>22</sup>, H. L. Ren<sup>18</sup>,  
M. Ripka<sup>22</sup>, G. Rong<sup>1</sup>, Ch. Rosner<sup>14</sup>, X. D. Ruan<sup>12</sup>, V. Santoro<sup>21A</sup>, A. Sarantsev<sup>23,g</sup>, M. Savrié<sup>21B</sup>, K. Schoenning<sup>49</sup>,  
S. Schumann<sup>22</sup>, W. Shan<sup>31</sup>, M. Shao<sup>45,a</sup>, C. P. Shen<sup>2</sup>, P. X. Shen<sup>30</sup>, X. Y. Shen<sup>1</sup>, H. Y. Sheng<sup>1</sup>, M. R. Shepherd<sup>19</sup>,  
W. M. Song<sup>1</sup>, X. Y. Song<sup>1</sup>, S. Sosio<sup>48A,48C</sup>, S. Spataro<sup>48A,48C</sup>, G. X. Sun<sup>1</sup>, J. F. Sun<sup>15</sup>, S. S. Sun<sup>1</sup>, Y. J. Sun<sup>45,a</sup>, Y. Z. Sun<sup>1</sup>,  
Z. J. Sun<sup>1,a</sup>, Z. T. Sun<sup>19</sup>, C. J. Tang<sup>36</sup>, X. Tang<sup>1</sup>, I. Tapan<sup>40C</sup>, E. H. Thorndike<sup>44</sup>, M. Tiemens<sup>25</sup>, D. Toth<sup>43</sup>, M. Ullrich<sup>24</sup>,  
I. Uman<sup>40B</sup>, G. S. Varner<sup>42</sup>, B. Wang<sup>30</sup>, B. L. Wang<sup>41</sup>, D. Wang<sup>31</sup>, D. Y. Wang<sup>31</sup>, K. Wang<sup>1,a</sup>, L. L. Wang<sup>1</sup>, L. S. Wang<sup>1</sup>,  
M. Wang<sup>33</sup>, P. Wang<sup>1</sup>, P. L. Wang<sup>1</sup>, S. G. Wang<sup>31</sup>, W. Wang<sup>1,a</sup>, X. F. Wang<sup>39</sup>, Y. D. Wang<sup>14</sup>, Y. F. Wang<sup>1,a</sup>, Y. Q. Wang<sup>22</sup>,  
Z. Wang<sup>1,a</sup>, Z. G. Wang<sup>1,a</sup>, Z. H. Wang<sup>45,a</sup>, Z. Y. Wang<sup>1</sup>, T. Weber<sup>22</sup>, D. H. Wei<sup>11</sup>, J. B. Wei<sup>31</sup>, P. Weidenkaff<sup>22</sup>, S. P. Wen<sup>1</sup>,  
U. Wiedner<sup>4</sup>, M. Wolke<sup>49</sup>, L. H. Wu<sup>1</sup>, Z. Wu<sup>1,a</sup>, L. G. Xia<sup>39</sup>, Y. Xia<sup>18</sup>, D. Xiao<sup>1</sup>, Z. J. Xiao<sup>28</sup>, Y. G. Xie<sup>1,a</sup>, Q. L. Xiu<sup>1,a</sup>,  
G. F. Xu<sup>1</sup>, L. Xu<sup>1</sup>, Q. J. Xu<sup>13</sup>, Q. N. Xu<sup>41</sup>, X. P. Xu<sup>37</sup>, L. Yan<sup>45,a</sup>, W. B. Yan<sup>45,a</sup>, W. C. Yan<sup>45,a</sup>, Y. H. Yan<sup>18</sup>, H. X. Yang<sup>1</sup>,  
L. Yang<sup>50</sup>, Y. Yang<sup>6</sup>, Y. X. Yang<sup>11</sup>, H. Ye<sup>1</sup>, M. Ye<sup>1,a</sup>, M. H. Ye<sup>7</sup>, J. H. Yin<sup>1</sup>, B. X. Yu<sup>1,a</sup>, C. X. Yu<sup>30</sup>, H. W. Yu<sup>31</sup>, J. S. Yu<sup>26</sup>,  
C. Z. Yuan<sup>1</sup>, W. L. Yuan<sup>29</sup>, Y. Yuan<sup>1</sup>, A. Yuncu<sup>40B,c</sup>, A. A. Zafar<sup>47</sup>, A. Zallo<sup>20A</sup>, Y. Zeng<sup>18</sup>, B. X. Zhang<sup>1</sup>, B. Y. Zhang<sup>1,a</sup>,  
C. Zhang<sup>29</sup>, C. C. Zhang<sup>1</sup>, D. H. Zhang<sup>1</sup>, H. H. Zhang<sup>38</sup>, H. Y. Zhang<sup>1,a</sup>, J. J. Zhang<sup>1</sup>, J. L. Zhang<sup>1</sup>, J. Q. Zhang<sup>1</sup>,  
J. W. Zhang<sup>1,a</sup>, J. Y. Zhang<sup>1</sup>, J. Z. Zhang<sup>1</sup>, K. Zhang<sup>1</sup>, L. Zhang<sup>1</sup>, S. H. Zhang<sup>1</sup>, X. Y. Zhang<sup>33</sup>, Y. Zhang<sup>1</sup>, Y. N. Zhang<sup>41</sup>,  
Y. H. Zhang<sup>1,a</sup>, Y. T. Zhang<sup>45,a</sup>, Yu Zhang<sup>41</sup>, Z. H. Zhang<sup>6</sup>, Z. P. Zhang<sup>45</sup>, Z. Y. Zhang<sup>50</sup>, G. Zhao<sup>1</sup>, J. W. Zhao<sup>1,a</sup>,  
J. Y. Zhao<sup>1</sup>, J. Z. Zhao<sup>1,a</sup>, Lei Zhao<sup>45,a</sup>, Ling Zhao<sup>1</sup>, M. G. Zhao<sup>30</sup>, Q. Zhao<sup>1</sup>, Q. W. Zhao<sup>1</sup>, S. J. Zhao<sup>52</sup>, T. C. Zhao<sup>1</sup>,  
Y. B. Zhao<sup>1,a</sup>, Z. G. Zhao<sup>45,a</sup>, A. Zhemchugov<sup>23,d</sup>, B. Zheng<sup>46</sup>, J. P. Zheng<sup>1,a</sup>, W. J. Zheng<sup>33</sup>, Y. H. Zheng<sup>41</sup>, B. Zhong<sup>28</sup>,  
L. Zhou<sup>1,a</sup>, Li Zhou<sup>30</sup>, X. Zhou<sup>50</sup>, X. K. Zhou<sup>45,a</sup>, X. R. Zhou<sup>45,a</sup>, X. Y. Zhou<sup>1</sup>, K. Zhu<sup>1</sup>, K. J. Zhu<sup>1,a</sup>, S. Zhu<sup>1</sup>, X. L. Zhu<sup>39</sup>,  
Y. C. Zhu<sup>45,a</sup>, Y. S. Zhu<sup>1</sup>, Z. A. Zhu<sup>1</sup>, J. Zhuang<sup>1,a</sup>, L. Zotti<sup>48A,48C</sup>, B. S. Zou<sup>1</sup>, J. H. Zou<sup>1</sup>

(BESIII Collaboration)

A. P. Szczepaniak<sup>19,53,54</sup>, P. Guo<sup>19,53</sup>

<sup>1</sup> Institute of High Energy Physics, Beijing 100049, People's Republic of China

<sup>2</sup> Beihang University, Beijing 100191, People's Republic of China

<sup>3</sup> Beijing Institute of Petrochemical Technology, Beijing 102617, People's Republic of China

<sup>4</sup> Bochum Ruhr-University, D-44780 Bochum, Germany

<sup>5</sup> Carnegie Mellon University, Pittsburgh, Pennsylvania 15213, USA

<sup>6</sup> Central China Normal University, Wuhan 430079, People's Republic of China

<sup>7</sup> China Center of Advanced Science and Technology, Beijing 100190, People's Republic of China

<sup>8</sup> COMSATS Institute of Information Technology, Lahore, Defence Road, Off Raiwind Road, 54000 Lahore, Pakistan

<sup>9</sup> G.I. Budker Institute of Nuclear Physics SB RAS (BINP), Novosibirsk 630090, Russia

<sup>10</sup> GSI Helmholtzcentre for Heavy Ion Research GmbH, D-64291 Darmstadt, Germany

- 61 <sup>11</sup> Guangxi Normal University, Guilin 541004, People's Republic of China  
62 <sup>12</sup> GuangXi University, Nanning 530004, People's Republic of China  
63 <sup>13</sup> Hangzhou Normal University, Hangzhou 310036, People's Republic of China  
64 <sup>14</sup> Helmholtz Institute Mainz, Johann-Joachim-Becher-Weg 45, D-55099 Mainz, Germany  
65 <sup>15</sup> Henan Normal University, Xinxiang 453007, People's Republic of China  
66 <sup>16</sup> Henan University of Science and Technology, Luoyang 471003, People's Republic of China  
67 <sup>17</sup> Huangshan College, Huangshan 245000, People's Republic of China  
68 <sup>18</sup> Hunan University, Changsha 410082, People's Republic of China  
69 <sup>19</sup> Indiana University, Bloomington, Indiana 47405, USA  
70 <sup>20</sup> (A)INFN Laboratori Nazionali di Frascati, I-00044, Frascati, Italy; (B)INFN and University of Perugia, I-06100, Perugia,  
71 Italy  
72 <sup>21</sup> (A)INFN Sezione di Ferrara, I-44122, Ferrara, Italy; (B)University of Ferrara, I-44122, Ferrara, Italy  
73 <sup>22</sup> Johannes Gutenberg University of Mainz, Johann-Joachim-Becher-Weg 45, D-55099 Mainz, Germany  
74 <sup>23</sup> Joint Institute for Nuclear Research, 141980 Dubna, Moscow region, Russia  
75 <sup>24</sup> Justus Liebig University Giessen, II. Physikalisches Institut, Heinrich-Buff-Ring 16, D-35392 Giessen, Germany  
76 <sup>25</sup> KVI-CART, University of Groningen, NL-9747 AA Groningen, The Netherlands  
77 <sup>26</sup> Lanzhou University, Lanzhou 730000, People's Republic of China  
78 <sup>27</sup> Liaoning University, Shenyang 110036, People's Republic of China  
79 <sup>28</sup> Nanjing Normal University, Nanjing 210023, People's Republic of China  
80 <sup>29</sup> Nanjing University, Nanjing 210093, People's Republic of China  
81 <sup>30</sup> Nankai University, Tianjin 300071, People's Republic of China  
82 <sup>31</sup> Peking University, Beijing 100871, People's Republic of China  
83 <sup>32</sup> Seoul National University, Seoul, 151-747 Korea  
84 <sup>33</sup> Shandong University, Jinan 250100, People's Republic of China  
85 <sup>34</sup> Shanghai Jiao Tong University, Shanghai 200240, People's Republic of China  
86 <sup>35</sup> Shanxi University, Taiyuan 030006, People's Republic of China  
87 <sup>36</sup> Sichuan University, Chengdu 610064, People's Republic of China  
88 <sup>37</sup> Soochow University, Suzhou 215006, People's Republic of China  
89 <sup>38</sup> Sun Yat-Sen University, Guangzhou 510275, People's Republic of China  
90 <sup>39</sup> Tsinghua University, Beijing 100084, People's Republic of China  
91 <sup>40</sup> (A)Istanbul Aydin University, 34295 Sefakoy, Istanbul, Turkey; (B)Dogus University, 34722 Istanbul, Turkey; (C)Uludag  
92 University, 16059 Bursa, Turkey  
93 <sup>41</sup> University of Chinese Academy of Sciences, Beijing 100049, People's Republic of China  
94 <sup>42</sup> University of Hawaii, Honolulu, Hawaii 96822, USA  
95 <sup>43</sup> University of Minnesota, Minneapolis, Minnesota 55455, USA  
96 <sup>44</sup> University of Rochester, Rochester, New York 14627, USA  
97 <sup>45</sup> University of Science and Technology of China, Hefei 230026, People's Republic of China  
98 <sup>46</sup> University of South China, Hengyang 421001, People's Republic of China  
99 <sup>47</sup> University of the Punjab, Lahore-54590, Pakistan  
100 <sup>48</sup> (A)University of Turin, I-10125, Turin, Italy; (B)University of Eastern Piedmont, I-15121, Alessandria, Italy; (C)INFN,  
101 I-10125, Turin, Italy  
102 <sup>49</sup> Uppsala University, Box 516, SE-75120 Uppsala, Sweden  
103 <sup>50</sup> Wuhan University, Wuhan 430072, People's Republic of China  
104 <sup>51</sup> Zhejiang University, Hangzhou 310027, People's Republic of China  
105 <sup>52</sup> Zhengzhou University, Zhengzhou 450001, People's Republic of China  
106 <sup>53</sup> Center for Exploration of Energy and Matter, Indiana University, Bloomington, IN 47403, USA  
107 <sup>54</sup> Theory Center, Thomas Jefferson National Accelerator Facility, Newport News, VA 23606, USA  
108 <sup>a</sup> Also at State Key Laboratory of Particle Detection and Electronics, Beijing 100049, Hefei 230026, People's Republic of  
109 China  
110 <sup>b</sup> Also at Ankara University, 06100 Tandogan, Ankara, Turkey  
111 <sup>c</sup> Also at Bogazici University, 34342 Istanbul, Turkey  
112 <sup>d</sup> Also at the Moscow Institute of Physics and Technology, Moscow 141700, Russia  
113 <sup>e</sup> Also at the Functional Electronics Laboratory, Tomsk State University, Tomsk, 634050, Russia  
114 <sup>f</sup> Also at the Novosibirsk State University, Novosibirsk, 630090, Russia  
115 <sup>g</sup> Also at the NRC "Kurchatov Institute, PNPI, 188300, Gatchina, Russia  
116 <sup>h</sup> Also at University of Texas at Dallas, Richardson, Texas 75083, USA  
117 <sup>i</sup> Currently at Istanbul Arel University, 34295 Istanbul, Turkey  
118 (Dated: June 1, 2015)

An amplitude analysis of the  $\pi^0\pi^0$  system produced in radiative  $J/\psi$  decays is presented. In particular, a piecewise function that describes the dynamics of the  $\pi^0\pi^0$  system is determined as a function of  $M_{\pi^0\pi^0}$  from an analysis of the  $(1.311 \pm 0.011) \times 10^9$   $J/\psi$  decays collected by the BESIII detector. The goal of this analysis is to provide a description of the scalar and tensor components of the  $\pi^0\pi^0$  system while making minimal assumptions about the properties or number of poles in the

amplitude. Such a model-independent description allows one to integrate these results with other related results from complementary reactions in the development of phenomenological models, which can then be used to directly fit experimental data to obtain parameters of interest. The branching fraction of  $J/\psi \rightarrow \gamma\pi^0\pi^0$  is determined to be  $(1.15 \pm 0.05) \times 10^{-3}$ , where the uncertainty is systematic only and the statistical uncertainty is negligible.

PACS numbers: 11.80.Et, 12.39.Mk, 13.20.Gd, 14.40.Be

## I. INTRODUCTION

While the Standard Model of particle physics has yielded remarkable successes, the connection between the quantum chromodynamics (QCD) and the complex structure of hadron dynamics remains elusive. The light isoscalar scalar meson spectrum ( $I^G J^{PC} = 0^+0^{++}$ ), for example, remains relatively poorly understood despite many years of investigation. This lack of understanding is due in part to the presence of broad, overlapping states, which are poorly described by the most accessible analytical methods (see the “Note on scalar mesons below 2 GeV” in the PDG) [1]. The PDG reports eight  $0^+0^{++}$  mesons, which have widths between 100 and 450 MeV. Several of these states, including the  $f_0(1370)$ , are characterized in the PDG only by ranges of values for their masses and widths.

Knowledge of the low mass scalar meson spectrum is important for several reasons. In particular, the lightest glueball state is expected to have scalar quantum numbers [2–5]. The existence of such a state is an excellent test of QCD. Experimental observation of a glueball state would provide evidence that gluon self-interactions can generate a massive meson. Unfortunately, glueballs may mix with conventional quark bound states, making the identification of glueball states experimentally challenging. The low mass scalar meson spectrum is also of interest in probing the fundamental interactions of hadrons in that it allows for testing of Chiral Perturbation Theory to one loop [6].

The scalar meson spectrum has been studied in many reactions, including  $\pi N$  scattering [7],  $p\bar{p}$  annihilation [8], central hadronic production [9], decays of the  $\psi'$  [10],  $J/\psi$  [11–13],  $B$  [14],  $D$  [15], and  $K$  [16] mesons,  $\gamma\gamma$  formation [17] and  $\phi$  radiative decays [18]. In particular, a coupled channel analysis using the K-matrix formalism has been performed using data from pion production,  $p\bar{p}$  and  $n\bar{p}$  annihilation, and  $\pi\pi$  scattering [19]. Similar investigations would benefit from the inclusion of data from radiative  $J/\psi$  decays, which provide a complementary source of hadronic production.

An attractive feature of a study of the two pseudoscalar spectrum in radiative  $J/\psi$  decays is the relative simplicity of the amplitude analysis. Conservation of parity in strong and electromagnetic interactions, along with the conservation of angular momentum, restricts the quantum numbers of the pseudoscalar-pseudoscalar pair. Only amplitudes with even angular momentum and positive parity and charge conjugation quantum numbers are accessible ( $J^{PC} = 0^{++}, 2^{++}, 4^{++}$ , etc). Initial studies

suggest that only the  $0^{++}$  and  $2^{++}$  amplitudes are significant in radiative  $J/\psi$  decays to  $\pi^0\pi^0$ . The neutral channel ( $\pi^0\pi^0$ ) is of particular interest due to the lack of sizable backgrounds like  $\rho\pi$ , which present a challenge for an analysis of the charged channel ( $\pi^+\pi^-$ ) [20].

Radiative  $J/\psi$  decays to  $\pi^+\pi^-$  have been analyzed previously by the MarkIII [21], DM2 [22], and BES [23] experiments. Decays to  $\pi^0\pi^0$  were also studied at Crystal Ball [24] and BES [25], but these analyses were severely limited by statistics, particularly for the higher mass states. Each of these analyses reported evidence for the  $f_2(1270)$  and some possible additional states near 1.710 GeV/ $c^2$  and 2.050 GeV/ $c^2$ . More recently, the BESII experiment studied these channels and implemented a partial wave analysis [20]. Prominent features in the results include the  $f_2(1270)$ ,  $f_0(1500)$ , and  $f_0(1710)$ . However, this analysis, like its predecessors, was limited by complications from large backgrounds and low statistics. Due to statistical limitations, the  $\pi^0\pi^0$  channel was used only as a cross check on the analysis of the charged channel.

Historically, amplitude analyses like that in Ref. [20] have relied on modeling the  $s$ -dependence of the  $\pi\pi$  interaction, where  $s$  is the invariant mass squared of the two pions, as a coherent sum of resonances, each described by a Breit-Wigner function. In doing so, a model is built whose parameters are resonance properties, e.g. masses, widths and branching fractions. A correspondence exists between these properties and the residues and poles of the  $\pi\pi$  scattering amplitude in the complex  $s$  plane; however, this correspondence is only valid in the limit of an isolated narrow resonance that is far from open thresholds (*cf.* Ref. [1]). For regions containing multiple overlapping resonances with large widths and the presence of thresholds, all of which occur in the  $0^{++}$   $\pi\pi$  spectrum, an amplitude constructed from a sum of Breit-Wigner functions becomes an approximation. While such an approximation provides a practical and controlled way to parameterize the data – additional resonances can be added to the sum until an adequate fit is achieved – it is unknown how well it maintains the correspondence between Breit-Wigner parameters and the analytic structure of the  $\pi\pi$  amplitude that one seeks to study, *i.e.*, the fundamental strong interaction physics. Often statistical precision, a lack of complementary constraining data, or a limited availability of models leaves the simple Breit-Wigner sum as a necessary but untested assumption in analyses, thereby rendering the numerical result only useful in the context of that assumption. In the context of this paper we refer to the Breit-Wigner sum

219 as a “mass dependent fit”, that is, the model used to fit  
220 the data has an assumed  $s$  dependence.

221 In this analysis we exploit the statistical precision pro-  
222 vided by  $(1.311 \pm 0.011) \times 10^9$   $J/\psi$  decays collected with  
223 the BESIII detector [26, 27] to measure the components  
224 of the  $\pi\pi$  amplitude independently for many small re-  
225 gions of  $\pi\pi$  invariant mass, which allows one to con-  
226 struct a piecewise complex function from the measure-  
227 ments that describes the  $s$ -dependence of the  $\pi\pi$  dy-  
228 namics. Such a construction makes minimal assumptions  
229 about the  $s$ -dependence of the  $\pi\pi$  interaction. We refer  
230 to this approach in the context of the paper as a “mass  
231 independent fit”.

232 The mass independent approach has some drawbacks.  
233 First, due to the large number of bins, one is left with  
234 a set of about a thousand parameters that describe the  
235 amplitudes with no single parameter tied to an individual  
236 resonance of interest. Second, mathematical ambiguities  
237 result in multiple sets of optimal parameters in each mass  
238 region. If only  $J = 0$  and  $J = 2$  resonances are signifi-  
239 cant, there are two ambiguous solutions. However, in  
240 general, if one includes  $J \geq 4$  the number of ambiguous  
241 solutions increases resulting in multiple allowed piecewise  
242 functions. Finally, in order to make the results practi-  
243 cally manageable for subsequent analysis, the assump-  
244 tion of Gaussian errors must be made – an assumption  
245 that cannot be validated in general. Similar limitations  
246 are present in other analyses of this type, *e.g.*, Ref. [7].  
247 In spite of these limitations, which are discussed further  
248 in Appendices B and C the results of the mass indepen-  
249 dent amplitude analysis presented here represent a mea-  
250 surement of  $\pi\pi$  dynamics in radiative  $J/\psi$  decays that  
251 minimizes experimental artifacts and potential system-  
252 atic biases due to theoretical assumptions. The results  
253 are presented with the intent of motivating the devel-  
254 opment of dynamical models with reaction independent  
255 parameters that can subsequently be optimized using ex-  
256 perimental data. All pertinent information for the use of  
257 these results in the study of pseudoscalar-pseudoscalar  
258 dynamics is included in the supplemental materials (Ap-  
259 pendix C).

## 260 II. THE BESIII DETECTOR

261 The Beijing Spectrometer (BESIII) is a general-  
262 purpose, hermetic detector located at the Beijing  
263 Electron-Positron Collider (BEPCII) in Beijing, China.  
264 BESIII and BEPCII represent major upgrades to the BE-  
265 SII detector and BEPC accelerator. The physics goals  
266 of the BESIII experiment cover a broad research pro-  
267 gram including charmonium physics, charm physics, light  
268 hadron spectroscopy and  $\tau$  physics, as well as searches  
269 for physics beyond the standard model. The detector  
270 is described in detail elsewhere [28]. A brief description  
271 follows.

272 The BESIII detector consists of five primary compo-  
273 nents working in conjunction to facilitate the reconstruc-

274 tion of events. A superconducting solenoid magnet pro-  
275 vides a uniform magnetic field within the detector. The  
276 field strength was 1.0 T during data collection in 2009,  
277 but was reduced to 0.9 T during the 2012 running period.  
278 Charged particle tracking is performed with a helium-gas  
279 based multilayer drift chamber (MDC). The momentum  
280 resolution of the MDC is expected to be better than 0.5%  
281 at 1 GeV/c, while the expected  $dE/dx$  resolution is 6%.  
282 With a timing resolution of 80 ps (110 ps) in the barrel  
283 (endcap), a plastic scintillator time-of-flight (TOF) de-  
284 tector is useful for particle identification. The energies of  
285 electromagnetic showers are determined using informa-  
286 tion from the electromagnetic calorimeter (EMC). The  
287 EMC consists of 6240 CsI(Tl) crystals arranged in one  
288 barrel and two endcap sections. With an angular cov-  
289 erage of about 93% of  $4\pi$ , the EMC provides an energy  
290 resolution of 2.5% (5%) at 1.0 GeV and a position resolu-  
291 tion of 6 mm (9 mm) in the barrel (endcap). Finally, par-  
292 ticles that escape these detectors travel through a muon  
293 chamber system (MUC), which provides additional infor-  
294 mation on the identity of particles. The MUC provides  
295 2 cm position resolution for muons and covers 89% of  
296  $4\pi$ . Muons with momenta over 0.5 GeV are detected  
297 with an efficiency greater than 90%. The efficiency of  
298 pions reaching the MUC is about 10% at this energy.

299 Selection criteria and background estimations are stud-  
300 ied using a GEANT4 Monte Carlo (MC) simulation. The  
301 BESIII Object Oriented Simulation Tool (BOOST) [29]  
302 provides a description of the geometry, material compo-  
303 sition, and detector response of the BESIII detector. The  
304 MC generator KKMC [30] is used for the production of  
305  $J/\psi$  mesons by  $e^+e^-$  annihilation, while BESEVTGEN [31]  
306 is used to generate the known decays of the  $J/\psi$  accord-  
307 ing to the world average values from the PDG [1]. The  
308 unknown portion of the  $J/\psi$  decay spectrum is generated  
309 with the Lundcharm model [32].

## 310 III. EVENT SELECTION

311 In order to be included in the amplitude analysis, an  
312 event must have at least five photon candidates and no  
313 charged track candidates. Any photon detected in the  
314 barrel (endcap) portion of the EMC must have an en-  
315 ergy of at least 25 (50) MeV. Four of the five photons are  
316 grouped into two pairs that may each originate from a  $\pi^0$   
317 decay. The invariant mass of any photon pair associated  
318 with a  $\pi^0$  must fall within 13 MeV/ $c^2$  of the  $\pi^0$  mass.  
319 A 6C kinematic fit is performed on each permutation of  
320 photons to the final state  $\gamma\pi^0\pi^0$ . This includes a con-  
321 straint on the four-momentum of the final state to that  
322 of the initial  $J/\psi$  (4C) and an additional constraint (1C)  
323 on each photon pair to have an invariant mass equal to  
324 that of a  $\pi^0$ .

325 Significant backgrounds in this channel include  $J/\psi$  de-  
326 cays to  $\gamma\eta$  ( $\eta \rightarrow \pi^0\pi^0\pi^0$ ) and  $\gamma\eta'$  ( $\eta' \rightarrow \eta\pi^0\pi^0; \eta \rightarrow \gamma\gamma$ ).  
327 Restricting the  $\chi^2$  from the 6C kinematic fit is an ef-  
328 fective means of reducing the backgrounds of this type.

Events with a  $\pi^0\pi^0$  invariant mass,  $M_{\pi^0\pi^0}$ , below KK threshold (the region in which these backgrounds are significant) must have a  $\chi^2$  less than 20. Events above KK threshold need only have a  $\chi^2$  less than 60. To reduce the background from  $J/\psi$  decays to  $\omega\pi^0$  ( $\omega \rightarrow \gamma\pi^0$ ), the invariant mass of each  $\gamma\pi^0$  pair is required to be at least 50 MeV/ $c^2$  away from the  $\omega$  mass [1]. Finally, in order to reduce the misreconstructed background arising from pairing the radiated photon with another photon in the event to form a  $\pi^0$ , the invariant mass of the radiated photon paired with any  $\pi^0$  daughter photon is required to be greater than 0.15 GeV/ $c^2$ .

If more than one permutation of five photons in an event satisfy these selection criteria, only the permutation with the minimum  $\chi^2$  from the 6C kinematic fit is retained. After all event selection criteria are applied, the number of events remaining in the data sample is 442,562. MC studies indicate that the remaining backgrounds exist at a level of about 1.8% of the size of the total sample. Table I lists the major backgrounds.

Backgrounds from  $J/\psi$  decays to  $\gamma\eta(\prime)$  are well understood and are studied with an exclusive MC sample, which is generated according to the PDG branching fractions for these reactions. Other backgrounds are studied using an inclusive MC sample generated using BESEVT-GEN, with the exception of the misreconstructed background, which is studied using an exclusive MC sample that resembles the data. The latter MC sample was generated using a set of Breit-Wigner resonances with couplings determined from a mass dependent fit to the data sample. The  $M_{\pi^0\pi^0}$  spectrum after all selection criteria have been applied is shown in Fig. 1. The reconstruction efficiency is determined to be 28.7%, according to the results of the mass independent amplitude analysis. Continuum backgrounds are investigated with a data sample collected at a center of mass energy of 3.080 GeV. The continuum backgrounds are scaled by luminosity and a correction factor for the difference in cross section as a function of center of mass energy. When scaled by luminosity, only 3,632 events, which represents approximately 0.8% of the signal, survive after all signal isolation requirements.

#### IV. AMPLITUDE ANALYSIS

##### A. General Formalism

The results of the mass independent amplitude analysis of the  $\pi^0\pi^0$  system are obtained from a series of unbinned extended maximum likelihood fits. The amplitudes for radiative  $J/\psi$  decays to  $\pi^0\pi^0$  are constructed in the radiative multipole basis, as described in detail in Appendix A.

Let  $U^{M,\lambda_\gamma}$  represent the amplitude for radiative  $J/\psi$  decays to  $\pi^0\pi^0$ ,

$$U^{M,\lambda_\gamma}(\vec{x}, s) = \langle \gamma\pi^0\pi^0 | H | J/\psi \rangle \quad (1)$$

TABLE I. The number of events remaining after all selection criteria for each of a number of background reactions is shown in the right column. The backgrounds are broken into three groups. The first group contains the signal mimicking decays. The second lists the remaining backgrounds from  $J/\psi$  decays to  $\gamma\eta(\prime)$ , while the third group lists a few additional backgrounds. The backgrounds explicitly listed here represent about 93% of the total background according to the MC samples. The misreconstructed background includes those events in which one of the daughter photons from a  $\pi^0$  decay is taken as the radiated photon.

Decay channel	Number of events
$J/\psi \rightarrow \gamma\pi^0\pi^0$ (data)	442,562
$e^+e^- \rightarrow \gamma\pi^0\pi^0$ (continuum)	3,632
$J/\psi \rightarrow b_1\pi^0; b_1 \rightarrow \gamma\pi^0$	1,606
$J/\psi \rightarrow \omega\pi^0; \omega \rightarrow \gamma\pi^0$	865
$J/\psi \rightarrow \rho\pi^0; \rho \rightarrow \gamma\pi^0$	778
Misreconstructed background	608
$J/\psi \rightarrow \gamma\eta; \eta \rightarrow 3\pi^0$	903
$J/\psi \rightarrow \gamma\eta'; \eta' \rightarrow \eta\pi^0\pi^0; \eta \rightarrow \gamma\gamma$	377
$J/\psi \rightarrow \omega\pi^0\pi^0; \omega \rightarrow \gamma\pi^0$	775
$J/\psi \rightarrow b_1\pi^0; b_1 \rightarrow \omega\pi^0; \omega \rightarrow \gamma\pi^0$	578
$J/\psi \rightarrow \omega\eta; \omega \rightarrow \gamma\pi^0$	409
$J/\psi \rightarrow \omega f_2(1270); \omega \rightarrow \gamma\pi^0$	299
$J/\psi \rightarrow \gamma\eta_c; \eta_c \rightarrow \gamma\pi^0\pi^0$ or $\pi^0\pi^0\pi^0$	255
Other backgrounds	507
Total Background (MC)	7,960

where  $\vec{x} = \{\theta_\gamma, \phi_\gamma, \theta_\pi, \phi_\pi\}$  is the position in phase space,  $s = M_{\pi^0\pi^0}^2$  is the invariant mass squared of the  $\pi^0\pi^0$  pair,  $M$  is the polarization of the  $J/\psi$ , and  $\lambda_\gamma$  is the helicity of the radiated photon. For the reaction under study the possible values of both  $M$  and  $\lambda_\gamma$  are  $\pm 1$ . The amplitude may be factorized into a piece that contains the radiative transition of the  $J/\psi$  to an intermediate state  $X$  and a piece that contains the QCD dynamics

$$U^{M,\lambda_\gamma}(\vec{x}, s) = \sum_{j, J_\gamma, X} \langle \pi^0\pi^0 | H_{QCD} | X_{j, J_\gamma} \rangle \times \langle \gamma X_{j, J_\gamma} | H_{EM} | J/\psi \rangle, \quad (2)$$

where  $j$  is the angular momentum of the intermediate state and  $J_\gamma$  indexes the radiative multipole transitions. The sum over  $X$  includes any pseudoscalar-pseudoscalar final states ( $\pi\pi$ ,  $K\bar{K}$ , etc) that may rescatter into  $\pi^0\pi^0$ . We assume that the contribution of the  $4\pi$  final state to this sum is negligible, with the result that rescattering effects become important only above the  $K\bar{K}$  threshold.

The amplitude in Eq. (2) may be further factorized by

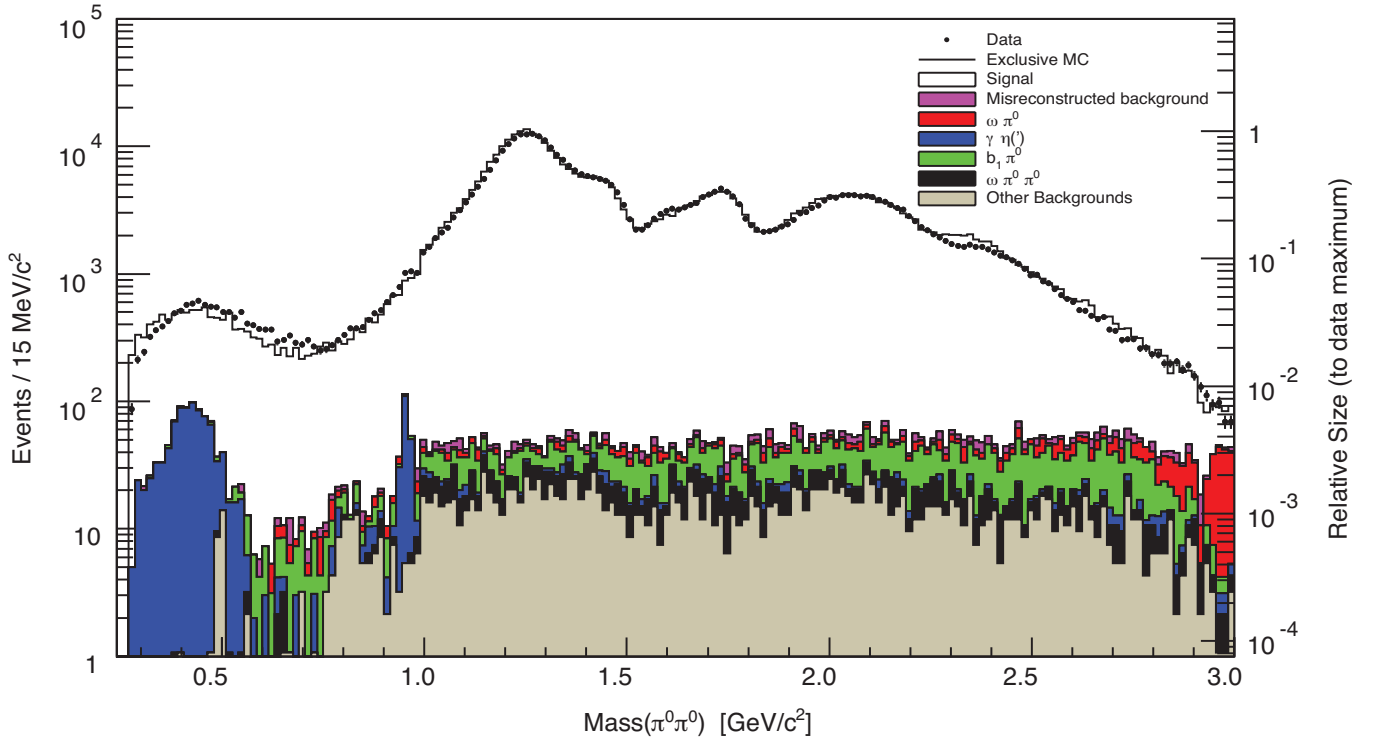


FIG. 1. The  $M_{\pi^0\pi^0}$  spectrum after all selection criteria have been applied. The black markers represent the data, while the histograms depict the backgrounds according to the MC samples. The signal (white) and misreconstructed background (pink) are determined from an exclusive MC sample that resembles the data. The other backgrounds are determined from an inclusive MC sample (see Table I). The components of the stacked histogram from bottom up are unspecified backgrounds,  $\omega\pi^0\pi^0$ ,  $b_1\pi^0$ ,  $\gamma\eta^{(\prime)}$ ,  $\omega\pi^0$ , the misreconstructed background, and the signal.

397 pulling out the angular distributions,

$$U^{M,\lambda_\gamma}(\vec{x}, s) = \sum_{j, J_\gamma, X} T_{j,X}(s) \Theta_j^{M,\lambda_\gamma}(\theta_\pi, \phi_\pi) \times g_{j, J_\gamma, X}(s) \Phi_{j, J_\gamma}^{M,\lambda_\gamma}(\theta_\gamma, \phi_\gamma), \quad (3)$$

398 where  $g_{j, J_\gamma, X}(s)$  is the coupling for the radiative decay  
 399 to intermediate state  $X$ . The functions  $\Theta_j^{M,\lambda_\gamma}(\theta_\pi, \phi_\pi)$   
 400 and  $\Phi_{j, J_\gamma}^{M,\lambda_\gamma}(\theta_\gamma, \phi_\gamma)$  contain the angular dependence of the  
 401 decay of the  $X$  to  $\pi^0\pi^0$  and the radiative  $J/\psi$  decay, respec-  
 402 tively. The part of the amplitude that describes the  
 403  $\pi^0\pi^0$  dynamics is the complex function  $T_{j,X}(s)$ , which is  
 404 of greatest interest for this study. However, this func-  
 405 tion cannot be separated from the coupling  $g_{j, J_\gamma, X}(s)$ .  
 406 Instead the product is measured according to

$$V_{j, J_\gamma}(s) \approx \sum_X g_{j, J_\gamma, X}(s) T_{j,X}(s). \quad (4)$$

407 This product will be called the coupling to the state with  
 408 characteristics  $j, J_\gamma$ . Note here that, if rescattering ef-  
 409 fects are assumed to be minimal (the only possible  $X$  is  
 410  $\pi\pi$ ), all amplitudes with the same  $j$  have the same phase.  
 411 The effect of rescattering is to break the factorizability

412 of Eq. (4). Finally, the amplitude may be written

$$U^{M,\lambda_\gamma}(\vec{x}, s) = \sum_{j, J_\gamma} V_{j, J_\gamma}(s) A_{j, J_\gamma}^{M,\lambda_\gamma}(\vec{x}), \quad (5)$$

413 where  $A_{j, J_\gamma}^{M,\lambda_\gamma}(\vec{x})$  contains the piece of the amplitude that  
 414 describes the angular distributions and is determined by  
 415 the kinematics of an event.

416 Any amplitude with total angular momentum greater  
 417 than zero will have three components (the  $0^{++}$  amplitude  
 418 has only an E1 component). Thus, three  $2^{++}$  amplitudes,  
 419 relating to E1, M2, and E3 radiative transitions, are in-  
 420 cluded in the analysis. While any amplitude with even  
 421 total angular momentum and positive parity and charge  
 422 conjugation is accessible for this decay, studies show that  
 423 the  $4^{++}$  amplitude is not significant in this region. In par-  
 424 ticular, no set of four continuous 15 MeV/ $c^2$  bins yield a  
 425 difference in  $-2 \ln L$  greater than 28.8 units, which corre-  
 426 sponds to a five sigma difference, under the inclusion of  
 427 a  $4^{++}$  amplitude. As no narrow spin-4 states are known,  
 428 this suggests that only the  $0^{++}$  and  $2^{++}$  amplitudes are  
 429 significant. The systematic uncertainty due to ignoring  
 430 a  $4^{++}$  amplitude that may exist in the data is described  
 431 below in Sec. V C.

## B. Parameterization

The dynamical function in Eq. (4) may be parameterized in various ways. A common parameterization, discussed in the introduction, is a sum of interfering Breit-Wigner functions,

$$V_{j,J_\gamma}(s) = \sum_{\beta} k_{j,J_\gamma,\beta} BW_{j,J_\gamma,\beta}(s), \quad (6)$$

where  $BW_{j,J_\gamma,\beta}(s)$  represents a Breit-Wigner function with characteristics (mass and width)  $\beta$  and strength  $k_{j,J_\gamma,\beta}$ .

To avoid making such a strong model dependent assumption, we choose to bin the data sample as a function of  $M_{\pi^0\pi^0}$  and to assume that the part of the amplitude that describes the dynamical function is constant over a small range of  $s$ ,

$$U^{M,\lambda_\gamma}(\vec{x}, s) = \sum_{j,J_\gamma} V_{j,J_\gamma} A_{j,J_\gamma}^{M,\lambda_\gamma}(\vec{x}). \quad (7)$$

For the scenario posed in Eq. (7), the couplings may be taken as the free parameters of an extended maximum likelihood fit in each bin of  $M_{\pi^0\pi^0}$ . It is then possible to extract a table of complex numbers (the free parameters in each bin) that describe the dynamical function of the  $\pi^0\pi^0$  interaction.

The intensity function,  $I(\vec{x})$ , which represents the density of events at some position in phase space  $\vec{x}$ , is given by

$$I(\vec{x}) = \sum_{M,\lambda_\gamma} \left| \sum_{j,J_\gamma} V_{j,J_\gamma} A_{j,J_\gamma}^{M,\lambda_\gamma}(\vec{x}) \right|^2. \quad (8)$$

The incoherent sum includes the observables of the reaction (which are not measured). For the reaction under study, the observables are the polarization of the  $J/\psi$ ,  $M = \pm 1$ , and the helicity of the radiated photon,  $\lambda_\gamma = \pm 1$ . The free parameters are constrained to be the same in each of the four pieces of the incoherent sum.

In the figures and supplemental results that follow, the intensity of the amplitude in each bin is reported as a number of events corrected for acceptance and detector efficiency. That is, for the bin of  $M_{\pi^0\pi^0}$  indexed by  $k$  and bounded by  $s_k$  and  $s_{k+1}$  (the boundaries in  $s$  of the bin) we report, for each amplitude indexed by  $j$  and  $J_\gamma$ , the quantity

$$I_{j,J_\gamma}^k = \int_{s_k}^{s_{k+1}} \sum_{M,\lambda_\gamma} \left| V_{j,J_\gamma}^k A_{j,J_\gamma}^{M,\lambda_\gamma}(\vec{x}) \right|^2 d\vec{x}. \quad (9)$$

In practice, we absorb the size of phase space into the fit parameters. In doing so we fit for parameters  $\tilde{V}_{j,J_\gamma}^k$  which are the  $V_{j,J_\gamma}^k$  scaled by the square root of the size of phase space in bin  $k$ .

## C. Background subtraction

The mass independent amplitude analysis treats each event in the data sample as a signal event. For a clean sample, the effect of remaining backgrounds should be small relative to the statistical errors on the amplitudes. However, the backgrounds from  $J/\psi$  decays to  $\gamma\eta(\prime)$  introduce a challenge. Both of these backgrounds peak in the low mass region near interesting structures. The background from  $J/\psi$  decays to  $\gamma\eta$  lies in the region of the  $f_0(500)$ , which is of particular interest for its importance to Chiral Perturbation Theory [1, 33]. The  $\gamma\eta'$  background peaks near the  $f_0(980)$ , which is also of particular interest due to its strong coupling to  $K\bar{K}$  and its implications for a scalar meson nonet [34]. Therefore, the effect of these backgrounds is removed by using a background subtraction method.

If a data sample is entirely free of backgrounds, the likelihood function is constructed as

$$L(\vec{\xi}) = \prod_{i=1}^{N_{\text{data}}^{\text{sig}}} f(\vec{x}_i|\vec{\xi}), \quad (10)$$

where  $f(\vec{x}|\vec{\xi})$  is the probability density function (pdf) to observe an event with a particular set of kinematics  $\vec{x}$  and parameters  $\vec{\xi} = \{\tilde{V}_{j,J_\gamma}^k\}$ . The total number of parameters in the mass independent analysis is 1,178 (seven times the number of bins above  $K\bar{K}$  threshold and five times the number of bins below  $K\bar{K}$  threshold). The number of events in the pure data sample is given by  $N_{\text{data}}^{\text{sig}}$ .

Now, the likelihood may be written

$$L(\vec{\xi}) = \prod_{i=1}^{N_{\text{data}}^{\text{sig}}} f(\vec{x}_i|\vec{\xi}) \prod_{j=1}^{N_{\text{data}}^{\text{bkg}}} f(\vec{x}_j|\vec{\xi}) \prod_{k=1}^{N_{\text{data}}^{\text{bkg}}} f(\vec{x}_k|\vec{\xi})^{-1}, \quad (11)$$

where an additional likelihood, which describes the reaction for background events, has been multiplied and divided. Consider now a more realistic data sample that consists not only of signal events, but also contains some number of background events,  $N_{\text{data}}^{\text{bkg}}$ . Then the product of the first two factors of Eq. (11) are simply the likelihood for the entire (contaminated) data sample, but the overall likelihood represents only that of the pure signal since the background likelihood has been divided. For a given data set, any backgrounds remaining after selection criteria have been applied are difficult to distinguish from the true signal. Rather than using the true background to determine the background likelihood, it is therefore necessary to approximate it with an exclusive MC sample. That is,

$$\prod_{i=1}^{N_{\text{data}}^{\text{bkg}}} f(\vec{x}_i|\vec{\xi})^{-1} \approx \prod_{i=1}^{N_{\text{MC}}^{\text{bkg}}} f(\vec{x}_i|\vec{\xi})^{-w_i}, \quad (12)$$

where the weight,  $w_i$ , is necessary for scaling purposes. For example, if the MC sample is twice the size of the

514 expected background, a weight factor of 0.5 is necessary.  
515 Finally, the likelihood function may be written

$$L(\vec{\xi}) = \prod_{i=1}^{N_{\text{data}}} f(\vec{x}_i|\vec{\xi}) \prod_{j=1}^{N_{\text{MC}}^{\text{bkg}}} f(\vec{x}_j|\vec{\xi})^{-w_j}. \quad (13)$$

516 In practice, this likelihood distribution is multiplied by  
517 a Poisson distribution for the extended maximum likeli-  
518 hood fits such that

$$L(\vec{\xi}) = \frac{e^{-\mu} \mu^{N_{\text{data}}}}{N_{\text{data}}!} \prod_{i=1}^{N_{\text{data}}} f(\vec{x}_i|\vec{\xi}) \prod_{j=1}^{N_{\text{MC}}^{\text{bkg}}} f(\vec{x}_j|\vec{\xi})^{-w_j}. \quad (14)$$

519 An exclusive MC sample for the backgrounds due to  
520  $J/\psi$  decays to  $\gamma\eta'$  is generated according to the branch-  
521 ing fractions given by the PDG [1]. This MC sample is  
522 required to pass all of the selection criteria that are ap-  
523 plied to the data sample. Any events that remain are  
524 included in the unbinned extended maximum likelihood  
525 fit with a negative weight ( $-w_j = -1$  in Eq. (13)). In this  
526 way, the inclusion of the MC sample in the fit approxi-  
527 mately cancels the effect of any remaining backgrounds  
528 of the same type in the data sample.

#### 529 D. Ambiguities

530 Another challenge to the amplitude analysis is the  
531 presence of ambiguities. Since the intensity function,  
532 which is fit to the data, is constructed from a sum of  
533 absolute squares, it is possible to identify multiple sets of  
534 amplitudes which give identical values for the total inten-  
535 sity. In this way, multiple solutions may give comparable  
536 values of  $-2 \ln L$  for a particular fit. For this particular  
537 analysis, two types of ambiguities are present. Trivial  
538 ambiguities arise due to the possibility of the overall am-  
539 plitude in each bin to be rotated by  $\pi$  or to be reflected  
540 over the real axis in the complex plane. These may be  
541 partially addressed by applying a phase convention to the  
542 results of the fits. Non-trivial ambiguities arise from the  
543 freedom of amplitudes with the same quantum numbers  
544 to have different phases. The non-trivial ambiguities rep-  
545 resent a greater challenge to the analysis and cannot be  
546 eliminated without introducing model dependencies.

547 While it is not possible in principle to measure the  
548 absolute phase of the amplitudes, it is possible to study  
549 the relative phases of individual amplitudes. Therefore in  
550 each of the fits, one of the amplitudes (the  $2^{++}$  E1 am-  
551 plitude) is constrained to be real. The phase difference be-  
552 tween the other amplitudes and that which is constrained  
553 can then be determined in each mass bin.

554 As mentioned above, a set of trivial ambiguities arises  
555 due to the possibility of the overall amplitude in each bin  
556 to be rotated by  $\pi$  or to be reflected over the real axis  
557 in the complex plane. Each of these processes leave the  
558 intensity distribution unchanged. This issue is partially  
559 resolved by establishing a phase convention in which the

560 amplitude that is constrained to be real is also con-  
561 strained to be positive. The remaining ambiguity is re-  
562 lated to the inability to determine the absolute phase.  
563 The phase of the total amplitude may change sign with-  
564 out inducing a change in the total intensity. Therefore,  
565 when a phase difference approaches zero, it is not pos-  
566 sible to determine if the phase difference should change  
567 sign. The amplitude analysis results are presented here  
568 with the arbitrary convention that the phase difference  
569 between the  $0^{++}$  amplitude and the  $2^{++}$  E1 amplitude is  
570 required to be positive. One may invert the sign of this  
571 phase difference in a given bin, but then all other phase  
572 differences in that bin must also be inverted.

573 The presence of non-trivial ambiguities is attributed to  
574 rescattering effects, which allow for amplitudes with the  
575 same quantum numbers,  $J^{PC}$ , to have different phases.  
576 The couplings,  $g_{j,J\gamma,X}(s)$ , in Eq. (4) are real functions  
577 of  $s$ . Since the dynamical amplitude,  $T_{j,X}(s)$ , does not  
578 depend on  $J_\gamma$ , its phase is the same for each of the am-  
579 plitudes with the same  $J^{PC}$  (in particular, the  $2^{++}$  E1,  
580 M2 and E3 amplitudes). However, if more than one in-  
581 termediate state,  $X$ , is present, differences between the  
582 couplings to these amplitudes may result in a phase dif-  
583 ference. Therefore, in the region above the  $K\bar{K}$  threshold  
584 the  $2^{++}$  amplitudes may have different phases. However,  
585 below  $K\bar{K}$  threshold the phases of these amplitudes are  
586 constrained to be the same. That is, rescattering through  
587  $4\pi$  is assumed to be negligible.

588 By writing out the angular dependence of the intensity  
589 function, it is possible to show that the freedom to have  
590 phase differences between the components of a given am-  
591 plitude ( $2^{++}$  E1, M2, and E3, for example) generates an  
592 ambiguity in the intensity distribution. For this chan-  
593 nel and considering only  $0^{++}$  and  $2^{++}$  amplitudes, two  
594 non-trivial ambiguous solutions may be present in each  
595 bin above  $K\bar{K}$  threshold. The knowledge of one solu-  
596 tion can be used to mathematically predict its ambiguous  
597 partner. In fact, some bins do not exhibit multiple so-  
598 lutions, but have a degenerate ambiguous pair. A study  
599 of these ambiguities (Appendix B) shows consistency be-  
600 tween the mathematically predicted and experimentally  
601 determined ambiguities. Both ambiguous solutions are  
602 presented, because it is impossible to know which rep-  
603 resent the physical solutions without making some addi-  
604 tional model dependent assumptions. If more than two  
605 solutions are found in a given bin, all solutions within 1  
606 unit of log likelihood from the best solution are compared  
607 to the predicted value *derived from the best solution* and  
608 only that which matches the prediction is accepted as the  
609 ambiguous partner.

#### 610 E. Results

##### 611 1. Amplitude intensities and phases

612 The intensity for each amplitude as a function of  $M_{\pi^0\pi^0}$   
613 is plotted in Fig. 2. Each of the phase differences with re-

spect to the reference amplitude ( $2^{++}$  E1), which is constrained to be real, is plotted in Fig. 3. Above the  $K\bar{K}$  threshold, two distinct sets of solutions are apparent in most bins as expected. The bins below about  $0.6 \text{ GeV}/c^2$  also contain multiple solutions, but with different likelihoods and are attributed to local minima in the likelihood function. The nominal solutions below  $0.6 \text{ GeV}/c^2$  are determined by requiring continuity in each intensity and phase difference as a function of  $M_{\pi^0\pi^0}$ . Only statistical errors are presented in the figures.

It is apparent that the ambiguous sets of solutions in the nominal results are distinct in some regions, while they approach and possibly cross at other points. The most powerful discriminator of this effect is the phase difference between the E1 and M2 components of the  $2^{++}$  amplitude (see the middle plot of Fig. 3). Regions in which the solutions may cross are apparent at  $0.99 \text{ GeV}/c^2$ , near  $1.3 \text{ GeV}/c^2$ , and above  $2.3 \text{ GeV}/c^2$ . Since the results in each bin are independent of their neighbor, it is not possible to identify two distinct, smooth solutions at these crossings.

## 2. Discussion

The results of the mass independent analysis exhibit significant structures in the  $0^{++}$  amplitude just below  $1.5 \text{ GeV}/c^2$  and near  $1.7 \text{ GeV}/c^2$ . This region is where one might expect to observe the the states  $f_0(1370)$ ,  $f_0(1500)$ , and  $f_0(1710)$  which are often cited as being mixtures of two scalar light quark states and a scalar glueball [35, 36]. A definitive statement on the number and properties of the scattering amplitude poles in this region of the spectrum requires model-dependent fits to the data. The effectiveness of any such model-dependent study could be greatly enhanced by including similar data from the decay  $J/\psi \rightarrow \gamma KK$  in an attempt to isolate production features from partial widths to  $KK$  and  $\pi\pi$  final states.

Additional structures are present in the  $0^{++}$  amplitude below  $0.6 \text{ GeV}/c^2$  and near  $2.0 \text{ GeV}/c^2$ . It seems reasonable to interpret the former as the  $\sigma$  ( $f_0(500)$ ). The latter could be attributed to the  $f_0(2020)$ . The presence of the four states below  $2.1 \text{ GeV}/c^2$  would be consistent with the previous study of radiative  $J/\psi$  decays to  $\pi\pi$  by BESII [20]. Finally, the results presented here also suggest two possible additional structures in the  $0^{++}$  spectrum that were not observed in Ref. [20]. These include a structure just below  $1 \text{ GeV}/c^2$ , which may indicate an  $f_0(980)$ , but the enhancement in this region is quite small. There also appears to be some structure in the  $0^{++}$  spectrum around  $2.4 \text{ GeV}/c^2$ .

In the  $2^{++}$  amplitude, the results of this analysis indicate a dominant contribution from what appears to be the  $f_2(1270)$ , consistent with previous results [20]. However, the remaining structure in the  $2^{++}$  amplitude appears significantly different than that assumed in the model used to obtain the BESII results [20]. In particu-

lar, the region between  $1.5$  and  $2.0 \text{ GeV}/c^2$  was described in the BESII analysis with a relatively narrow  $f_2(1810)$ . One permutation of the nominal results (the red markers in Fig. 2) indicates that the structures in this region are much broader, while the other permutation (the black markers in Fig. 2) suggests that there is very little contribution from any  $2^{++}$  states in this region.

The tensor spectrum near  $2 \text{ GeV}/c^2$  is of interest in the search for a tensor glueball. Previous investigations of the  $J/\psi \rightarrow \gamma\pi^0\pi^0$  channel reported evidence for a narrow ( $\Gamma \approx 20 \text{ MeV}$ ) tensor glueball candidate,  $f_J(2230)$  [25]. While a model-dependent fit is required to place a limit on the production of such a state using these data, we note that based on the reported value of  $B(J/\psi \rightarrow \gamma f_J(2230))$  [23], one would naively expect to observe a peak for the  $f_J(2230)$  with an integral that is of order  $4 \times 10^5$  but concentrated only in roughly two bins of  $M(\pi^0\pi^0)$ , corresponding to the full width of the  $f_J(2230)$ . Such a structure seems difficult to accommodate in the extracted  $2^{++}$  amplitude.

## F. Branching fraction

The results of the mass independent amplitude analysis allow for a measurement of the branching fraction of radiative  $J/\psi$  decays to  $\pi^0\pi^0$ , which is determined according to:

$$\mathcal{B}(J/\psi \rightarrow \gamma\pi^0\pi^0) = \frac{N_{\gamma\pi^0\pi^0} - N_{\text{bkg}}}{\epsilon_\gamma N_{J/\psi}}, \quad (15)$$

where  $N_{\gamma\pi^0\pi^0}$  is the number of acceptance corrected events,  $N_{\text{bkg}}$  is the number of remaining background events,  $\epsilon_\gamma$  is an efficiency correction necessary to extrapolate the  $\pi^0\pi^0$  spectrum down to a radiative photon energy of zero, and  $N_{J/\psi}$  is the number of  $J/\psi$  decays in the data. The number of acceptance corrected events is determined from the amplitude analysis by summing the total intensity from each  $M_{\pi^0\pi^0}$  bin. The number of remaining background events is determined according to the inclusive and exclusive MC samples. The fractional background contamination in each bin  $i$ ,  $R_{\text{bkg},i}$ , is determined before acceptance correction. The number of background events is then determined by assuming  $R_{\text{bkg},i}$  is constant after acceptance correction such that the number of background events in bin  $i$ ,  $N_{\text{bkg},i}$ , is given by the product of  $R_{\text{bkg},i}$  and the number of acceptance corrected events in the same bin,  $N_{\gamma\pi^0\pi^0,i}$ . Note that the backgrounds from  $J/\psi$  decays to  $\gamma\eta(\prime)$  are removed during the fitting process and are not included in this factor. The efficiency correction factor,  $\epsilon_\gamma$ , is determined by calculating the fraction of phase space that is removed by applying the selection requirements on the energy of the radiative photon. This extrapolation increases the total number of events by  $0.07\%$ . Therefore,  $\epsilon_\gamma$  is taken to be  $0.9993$ .

The backgrounds remaining after event selection fall into three categories. The misreconstructed backgrounds

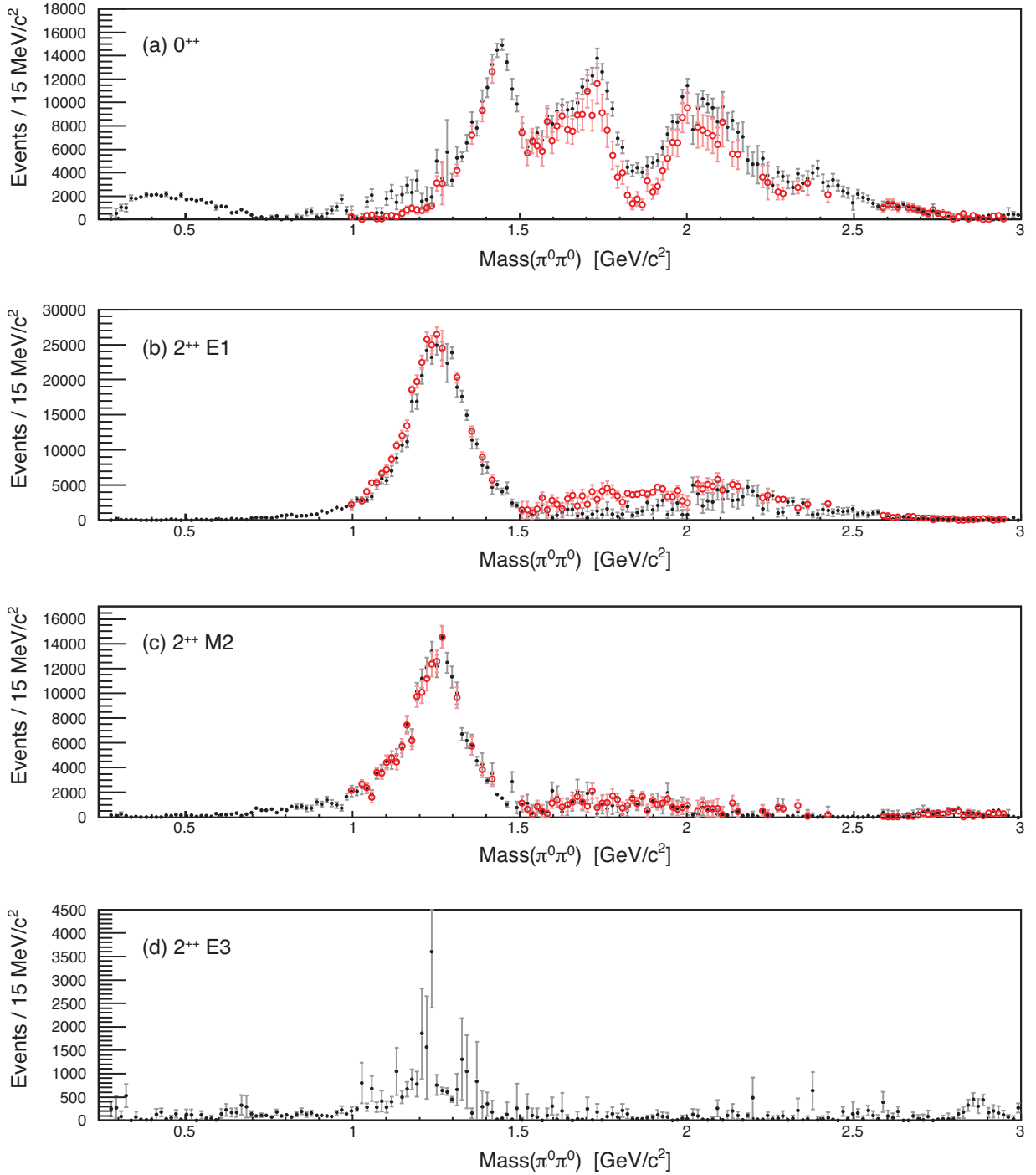


FIG. 2. The intensities for the (a)  $0^{++}$ , (b)  $2^{++}$  E1, (c)  $2^{++}$  M2 and (d)  $2^{++}$  E3 amplitudes as a function of  $M_{\pi^0\pi^0}$  for the nominal results. The solid black markers show the intensity calculated from one set of solutions, while the open red markers represent its ambiguous partner. Note that the intensity of the  $2^{++}$  E3 amplitude is redundant for the two ambiguous solutions (see Appendix B). Only statistical errors are presented.

721 are determined from an exclusive MC sample that re- 726 using the inclusive MC sample. Each of these back-  
 722 sembles the data. Events that remain in a continuum 727 grounds is scaled appropriately. In total, the acceptance  
 723 data sample taken at 3.080 GeV after selection criteria 728 corrected number of background events,  $N_{\text{bkg}}$ , is deter-  
 724 have been applied are also taken as a background. Fi- 729 mined to be 35,951. The number of radiative  $J/\psi$  decays  
 725 nally, the other remaining backgrounds are determined 730 to  $\pi^0\pi^0$ ,  $N_{\gamma\pi^0\pi^0}$ , is determined to be 1,543,050 events.

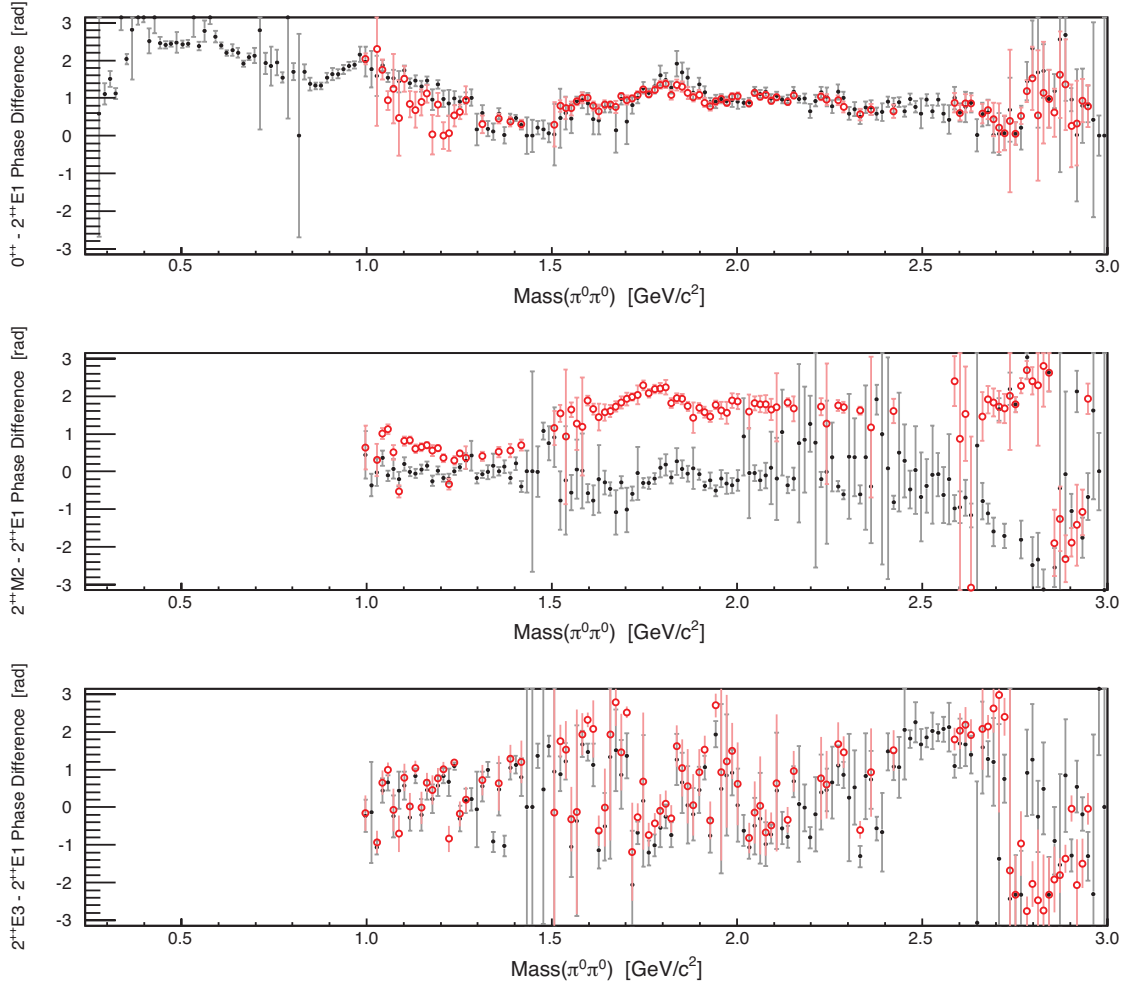


FIG. 3. The phase differences relative to the reference amplitude ( $2^{++}$  E1) for the (a)  $0^{++}$ , (b)  $2^{++}$  M2, and (c)  $2^{++}$  E3 amplitudes as a function of  $M_{\pi^0\pi^0}$  for the nominal results. The solid black markers show the phase differences calculated from one set of solutions, while the open red markers represent the ambiguous partner solutions. An arbitrary phase convention is applied here in which the phase difference between the  $0^{++}$  and  $2^{++}$  E1 amplitudes is required to be positive. Only statistical errors are presented.

731 The branching fraction for this decay is then determined  
 732 to be  $(1.151 \pm 0.002) \times 10^{-3}$ , where the error is statistical  
 733 only.

## 734 V. SYSTEMATIC UNCERTAINTIES

735 The systematic uncertainties for the mass independent  
 736 analysis include two types. First, the uncertainty due  
 737 to the effect of backgrounds from  $J/\psi$  decays to  $\gamma\eta(\prime)$   
 738 are addressed by repeating the analysis and treating the  
 739 background in a different manner. The second type of  
 740 systematic uncertainty is that due to the overall normal-  
 741 ization of the results. Sources of systematic uncertainties  
 742 of this type include the photon detection efficiency, the  
 743 total number of  $J/\psi$  decays, the effect of various back-  
 744 grounds, differences in the effect of the kinematic fit be-  
 745 tween the data and MC samples and the effect of model

746 dependencies. The uncertainty on the branching fraction  
 747 of  $\pi^0$  to  $\gamma\gamma$  according to the PDG is 0.03% [1], which  
 748 is negligible in relation to the other sources of uncer-  
 749 tainty. The systematic uncertainties are described below  
 750 and summarized in Table II. These uncertainties also  
 751 apply to the branching fraction measurement. Finally,  
 752 several cross checks are also performed.

### A. $J/\psi \rightarrow \gamma\eta$ and $J/\psi \rightarrow \gamma\eta'$ Background Uncertainty

753 The amplitude analysis is performed with the assump-  
 754 tion that all backgrounds have been eliminated. Stud-  
 755 ies using Monte Carlo simulation indicate this is a valid  
 756 assumption for most of the  $M_{\pi^0\pi^0}$  spectrum. However,  
 757 significant backgrounds from  $J/\psi$  decays to  $\gamma\eta$  and  $\gamma\eta'$   
 758 exist in many mass bins below about 1  $\text{GeV}/c^2$ . Rather  
 759  
 760

761 than inflating the errors of these bins according to the un- 815  
 762 certainty introduced by these backgrounds, which would 816  
 763 not take into account the bin-to-bin correlations, a set 817  
 764 of alternate results is presented in which the  $\gamma\eta(')$  back- 818  
 765 grounds are not subtracted. 819

766 The fraction of events in  $J/\psi$  decays to  $\gamma\eta(')$  that sur- 820  
 767 vive the event selection criteria for the  $\gamma\pi^0\pi^0$  final state 821  
 768 is very small (about 0.02%). Minor changes to the mod- 822  
 769 eling of these decays may therefore have a large effect 823  
 770 on the backgrounds. The difference between the nominal 824  
 771 results and the alternate results, which treat the back-  
 772 grounds differently, can be viewed as an estimator of the  
 773 systematic error in the results due to these backgrounds.

774 The distinctive feature of the alternate results is an  
 775 enhancement in the  $0^{++}$  intensity in the region below  
 776 about 0.6 GeV/ $c^2$  and near the  $\eta'$  peak. This may be  
 777 interpreted as the contribution of the events from  $J/\psi$   
 778 decays to  $\gamma\eta(')$ , which are being treated as signal events.  
 779 A comparison of the  $0^{++}$  amplitude for nominal results  
 780 and the alternate results is presented in Fig. 4. The re-  
 781 sults for the other amplitudes are consistent between the  
 782 two methods. Any conclusion drawn from these data  
 783 that is sensitive to choosing specifically the alternate or  
 784 nominal results is not a robust conclusion.

## 785 B. Uncertainties in the overall normalization

### 786 1. Photon Detection Efficiency

787 The primary source of systematic uncertainty for this  
 788 analysis comes from the reconstruction of photons. To  
 789 account for this uncertainty, the photon detection effi-  
 790 ciency of the BESIII detector is studied using the so  
 791 called tag and probe method on a sample of  $J/\psi$  de-  
 792 cays to  $\pi^+\pi^-\pi^0$ , where the  $\pi^0$  decays into two photons.  
 793 One of these final state photons is reconstructed, along  
 794 with the two charged tracks, while the other photon is  
 795 left as a missing particle in the event. This information  
 796 can then be used to determine the region in the detec-  
 797 tor where the missing photon is expected. The photon  
 798 detection efficiency is calculated by taking the ratio of  
 799 the number of missing photons that are detected in this  
 800 region to the number that are expected. The numbers of  
 801 detected and expected photons are determined with fits  
 802 to the two photon invariant mass distributions.

803 The systematic uncertainty due to photon reconstruc-  
 804 tion is determined by investigating the differences be-  
 805 tween the photon detection efficiencies of the inclusive  
 806 MC sample and that of the data sample. This difference  
 807 is measured to be less than 1.0%, which is taken to be  
 808 the systematic uncertainty per photon. For the five pho-  
 809 ton final state the overall uncertainty due to this effect  
 810 is therefore taken to be 5.0%.

811 An additional source of uncertainty, which is due to  
 812 mismodelling of the photon detection efficiency as a func-  
 813 tion of the angular and energy dependence of the radi-  
 814 ative photon, was studied using the same channel. The

815 phase space MC samples used for normalization in each  
 816 bin of the mass independent amplitude analysis were  
 817 modified to account for differences in the photon detec-  
 818 tion efficiency between the data and inclusive MC sam-  
 819 ples. The mass independent analysis was then repeated  
 820 using the modified phase space MC samples. Neither the  
 821 differences in angular nor energy dependence had a sig-  
 822 nificant effect on the results of the analysis. The effects  
 823 of mismodelling of this type are therefore taken to be  
 824 negligible.

### 825 2. Number of $J/\psi$

826 The number of  $J/\psi$  decays is determined from an anal-  
 827 ysis of inclusive hadronic events

$$N_{J/\psi} = \frac{N_{\text{sel}} - N_{\text{bg}}}{\epsilon_{\text{trig}} \times \epsilon_{\text{data}}^{\psi(2S)} \times f_{\text{cor}}}, \quad (16)$$

828 where  $N_{\text{sel}}$  represents the number of inclusive events re-  
 829 maining after selection criteria have been applied and  
 830  $N_{\text{bg}}$  is the number of background events estimated with a  
 831 data sample collected at 3.080 GeV. The efficiency for the  
 832 trigger is given by  $\epsilon_{\text{trig}}$ , while  $\epsilon_{\text{data}}^{\psi(2S)}$  is the detection ef-  
 833 ficiency for  $J/\psi$  inclusive decays determined from  $\psi(2S)$   
 834 decays to  $\pi^+\pi^-J/\psi$ . Finally,  $f_{\text{cor}}$  represents a correction  
 835 factor to translate  $\epsilon_{\text{data}}^{\psi(2S)}$  to the efficiency for inclusive de-  
 836 cays in which the  $J/\psi$  is produced at rest. To obtain  $N_{\text{sel}}$ ,  
 837 at least two charged tracks are required for each event.  
 838 Additionally, the momenta of these tracks and the visible  
 839 energy of each event are restricted in order to eliminate  
 840 Bhabha and di-muon events as well as beam gas inter-  
 841 actions and virtual photon-photon collisions. The total  
 842 number of  $J/\psi$  decays in the data sample according to  
 843 Eq. (16) is determined to be  $(1.311 \pm 0.011) \times 10^9$  events,  
 844 which results in an uncertainty of 0.8% [26, 27].

### 845 3. Background Size

846 According to the inclusive MC sample, the total num-  
 847 ber of background events that contaminate the signal is  
 848 about 1.5%. These do not include the misreconstructed  
 849 backgrounds nor the backgrounds from  $J/\psi$  decays to  
 850  $\gamma\eta(')$ , both of which are addressed in a separate system-  
 851 atic uncertainty. Additionally, backgrounds from non-  
 852  $J/\psi$  decays yield a contamination of approximately 0.8%.  
 853 Conservative systematic uncertainties equal to 100% of  
 854 the background contamination are attributed to each of  
 855 the inclusive MC and continuum background types.

### 856 4. Uncertainty in the acceptance corrected signal yield

857 One of the largest remaining backgrounds after signal  
 858 isolation and background subtraction is the signal mim-  
 859 icking decay of  $J/\psi$  to  $\omega\pi^0$ , where the  $\omega$  decays to  $\gamma\pi^0$ .

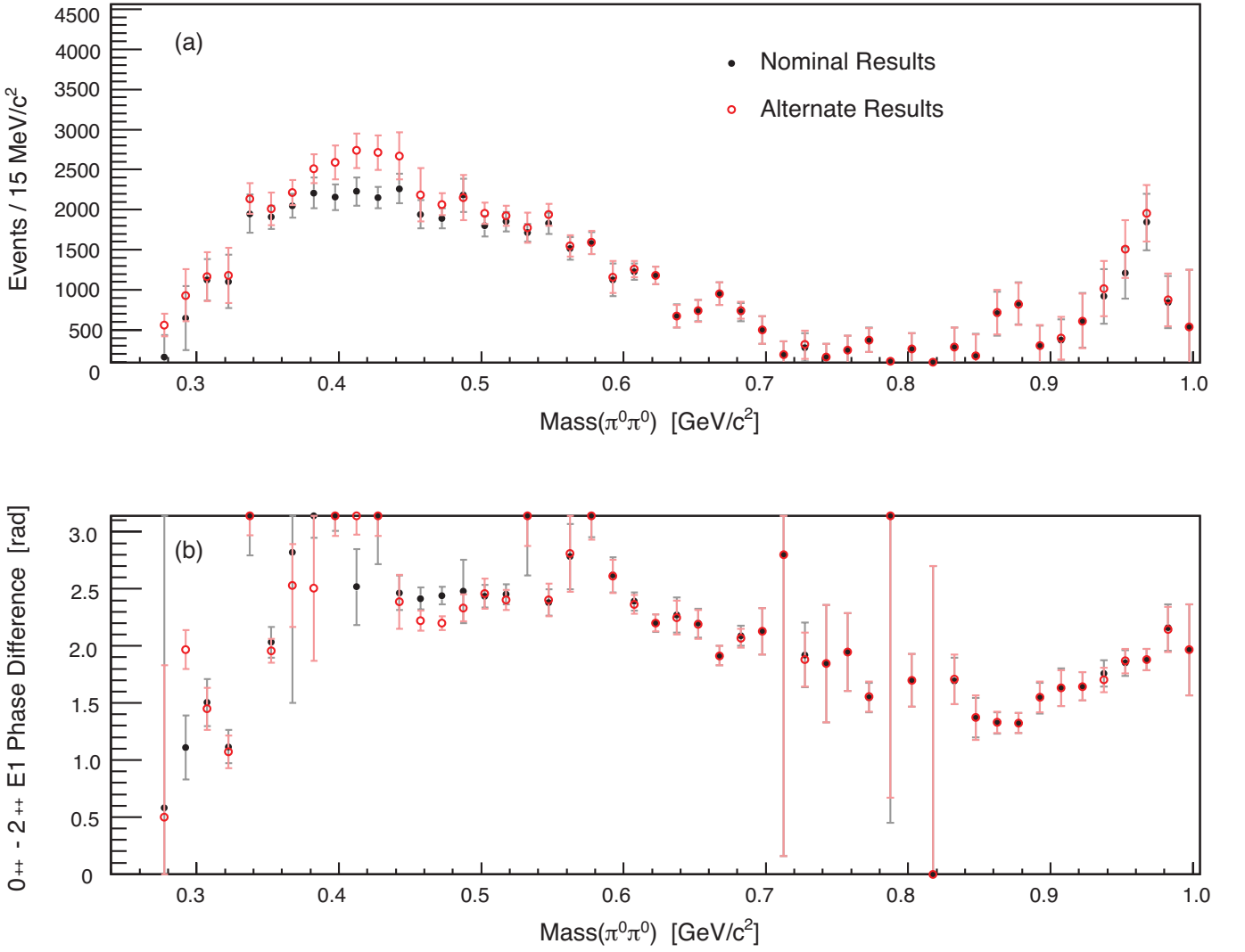


FIG. 4. A comparison of the (a)  $0^{++}$  intensity and (b) phase difference relative to the  $2^{++}$  E1 amplitude for the nominal results and the alternate results, in which the  $\gamma\eta(\prime)$  backgrounds have not been subtracted from the data. The solid black markers show the nominal results, while the red markers represent the alternate results. Only statistical errors are presented.

860 The nominal method to address this background is to re- 878  
 861 strict the  $\gamma\pi^0$  invariant mass to exclude the region within 879  
 862 50 MeV/c<sup>2</sup> of the  $\omega$  mass. An alternative method is to in- 880  
 863 clude an amplitude for the  $\omega\pi^0$  final state in the analysis. 881  
 864 The results of this alternative method are quantitatively 882  
 865 no different than the nominal results, suggesting that the 883  
 866 exclusion method is an effective means of addressing the 884  
 867 background from  $J/\psi$  decays to  $\omega\pi^0$ . The difference in 885  
 868 the branching fraction using the signal yield for the alter- 886  
 869 native method compared to the nominal method is about 887  
 870 0.8%. 888

871 As discussed above, backgrounds due to  $J/\psi$  decays 889  
 872 to  $\gamma\eta(\prime)$  are addressed in the fitting procedure itself by 890  
 873 adding an exclusive MC sample to the data, but with a 891  
 874 negative weight. The systematic uncertainty do to this 892  
 875 background is determined by using the data alone. In this 893  
 876 way, contributions from these backgrounds are treated as 894  
 877 signal and inflate the signal yield and background size 895

in Eq. (15). The difference in the branching fraction is 879  
 0.03%, which is considered a negligible contribution to 880  
 the systematic uncertainty.

Differences in the effect of the 6C kinematic fit on the 881  
 data and MC samples may cause a systematic difference 882  
 in the acceptance corrected signal yield. This effect was 883  
 investigated by loosening the restriction on the  $\chi^2$  from 884  
 the 6C kinematic fit. For events with a  $M_{\pi^0\pi^0}$  above 885  
 KK threshold, this restriction was relaxed from less than 886  
 60 to be less than 125. Events with an invariant mass 887  
 below KK threshold are required to have a  $\chi^2$  less than 60 888  
 rather than less than 20. The difference in the branching 889  
 fraction for the results with the loosened  $\chi^2$  cut relative 890  
 to that of the nominal results is about 0.1%. 891

892 Another source of systematic uncertainty in the 893  
 894 branching fraction is the difference between the nomi- 894  
 895 nal results and those obtained by applying a model that 895  
 describes the  $\pi\pi$  dynamics. To test this effect, a mass

dependent fit using interfering Breit-Wigner line shapes was performed. The difference in the branching fraction using the acceptance corrected yield of the mass dependent analysis compared to the nominal results is about 0.3%.

The effect of the remaining misreconstructed backgrounds on the results is studied by performing a closure test, in which the mass independent amplitude analysis is performed on an exclusive MC sample. This MC sample was generated according to the results of a mass dependent amplitude analysis of the data and includes the proper angular distributions. After applying the same selection criteria that are applied to the data, the MC sample is passed through the mass independent analysis. This process is repeated after removing the remaining misreconstructed backgrounds from the sample. The difference in the branching fraction between these two methods is 0.01%. The effect of these backgrounds is therefore taken to be negligible.

TABLE II. This table summarizes the systematic uncertainties (in %) for the branching fraction of radiative  $J/\psi$  decays to  $\pi^0\pi^0$ .

Source	$J/\psi \rightarrow \gamma\pi^0\pi^0$ (%)
Photon detection efficiency	5.0
Number of $J/\psi$	0.8
Inclusive MC backgrounds	1.5
Non- $J/\psi$ backgrounds	0.8
$\omega\pi^0$ background	0.8
Kinematic fit $\chi^2_{6C}$	0.1
Model dependent comparison	0.3
Total	5.4

### C. $4^{++}$ amplitude

As discussed above, the only  $\pi^0\pi^0$  amplitudes that are accessible in radiative  $J/\psi$  decays have even angular momentum and positive parity and charge conjugation quantum numbers. The mass independent analysis was performed under the assumption that only the  $0^{++}$  and  $2^{++}$  amplitudes are significant. To test this assumption, the analysis was repeated with the addition of a  $4^{++}$  amplitude. No significant contribution from a  $4^{++}$  amplitude is apparent.

To test the effect of a  $4^{++}$  amplitude that may exist in the data and is ignored in the fit, an exclusive MC sample was generated using a model constructed from a sum of resonances each parameterized by a Breit-Wigner function in a way that optimally reproduces the data. One of the resonances was an  $f_4(2050)$ , which was generated in each component of the  $4^{++}$  amplitude. The relative size of the  $4^{++}$  amplitude was determined from a mass dependent fit to the data, in which the  $4^{++}$  amplitude contributed 0.43% to the overall intensity. A mass inde-

pendent amplitude analysis, which did not include a  $4^{++}$  amplitude, was then performed on this sample. The results indicate that the intensities and phases for the  $0^{++}$  and  $2^{++}$  amplitudes deviate from the input parameters at the order of the statistical errors from the data sample in the region between 1.5 and 3.0 GeV/ $c^2$ . Therefore, the systematic error due to the effect of ignoring a possible  $4^{++}$  amplitude is estimated to be of the same order as the statistical errors in the region from 1.5 to 3.0 GeV/ $c^2$ .

## VI. CONCLUSIONS

A mass independent amplitude analysis of the  $\pi^0\pi^0$  system in radiative  $J/\psi$  decays is presented. This analysis uses the world's largest data sample of its type, collected with the BESIII detector, to extract a piecewise function that describes the scalar and tensor  $\pi\pi$  amplitudes in this decay. While the analysis strategy employed to obtain results has complications, namely ambiguous solutions, a large number of parameters, and potential bias in subsequent analyses from non-Gaussian effects (see Appendix C), it minimizes systematic bias arising from assumptions about  $\pi\pi$  dynamics, and, consequently, permits the development of dynamical models or parameterizations for the data.

In order to facilitate the development of models, the results of the mass independent analysis are presented in two ways. The intensities and phase differences for the amplitudes in the fit are presented here as a function of  $M_{\pi^0\pi^0}$ . Additionally, the intensities and phases for each bin of  $M_{\pi^0\pi^0}$  are given in supplemental materials (see Appendix C). These results may be combined with those of similar reactions for a more comprehensive study of the light scalar meson spectrum. Finally, the branching fraction of radiative  $J/\psi$  decays to  $\pi^0\pi^0$  is measured to be  $(1.15 \pm 0.05) \times 10^{-3}$ , where the error is systematic only and the statistical error is negligible. This is the first measurement of this branching fraction.

## ACKNOWLEDGMENTS

The BESIII collaboration thanks the staff of BEPCII and the IHEP computing center for their strong support. This work is supported in part by National Key Basic Research Program of China under Contract No. 2015CB856700; National Natural Science Foundation of China (NSFC) under Contracts Nos. 11125525, 11235011, 11322544, 11335008, 11425524; the Chinese Academy of Sciences (CAS) Large-Scale Scientific Facility Program; the CAS Center for Excellence in Particle Physics (CCEPP); the Collaborative Innovation Center for Particles and Interactions (CICPI); Joint Large-Scale Scientific Facility Funds of the NSFC and CAS under Contracts Nos. 11179007, U1232201, U1332201; CAS under Contracts Nos. KJCX2-YW-N29, KJCX2-YW-N45; 100 Talents Program of CAS; INPAC and Shanghai Key

987 Laboratory for Particle Physics and Cosmology; German  
 988 Research Foundation DFG under Contract No. Collab-  
 989 orative Research Center CRC-1044; Istituto Nazionale  
 990 di Fisica Nucleare, Italy; Ministry of Development of  
 991 Turkey under Contract No. DPT2006K-120470; Russian  
 992 Foundation for Basic Research under Contract No. 14-  
 993 07-91152; U. S. Department of Energy under Contracts  
 994 Nos. DE-FG02-04ER41291, DE-FG02-05ER41374, DE-  
 995 FG02-94ER40823, DESC0010118; U.S. National Sci-  
 996 ence Foundation; University of Groningen (RuG) and  
 997 the Helmholtzzentrum fuer Schwerionenforschung GmbH  
 998 (GSI), Darmstadt; WCU Program of National Research  
 999 Foundation of Korea under Contract No. R32-2008-000-  
 1000 10155-0; U.S. Department of Energy under Grant No.  
 1001 DE-FG02-87ER40365. This research was supported in  
 1002 part by Lilly Endowment, Inc., through its support for  
 1003 the Indiana University Pervasive Technology Institute,  
 1004 and in part by the Indiana METACyt Initiative. The

1005 Indiana METACyt Initiative at IU is also supported in  
 1006 part by Lilly Endowment, Inc.

## Appendix A: Amplitudes

1008 The amplitude for radiative  $J/\psi$  decays to  $\pi^0\pi^0$  can  
 1009 be determined in different bases depending on the infor-  
 1010 mation of interest. For example, in the helicity basis,  
 1011 the amplitude depends on the angular momentum and  
 1012 helicity of the  $\pi^0\pi^0$  resonance as well as the angular mo-  
 1013 mentum and polarization of the  $J/\psi$ . It is also possible to  
 1014 relate the amplitudes to radiative multipole transitions.  
 1015 Such a basis is useful because it may allow implementa-  
 1016 tion or testing of dynamical assumptions. For example,  
 1017 a model may suggest that the E1 radiative transition  
 1018 should dominate over the M2 transition.

1019 In the radiative multipole basis, the amplitude for ra-  
 1020 diative  $J/\psi$  decays to  $\pi^0\pi^0$  is given by

$$\begin{aligned}
 U^{M,\lambda_\gamma}(\vec{x}, s) &= \sum_{j, J_\gamma, \mu} N_{J_\gamma} N_j D_{M, \mu - \lambda_\gamma}^J(\pi + \phi_\gamma, \pi - \theta_\gamma, 0) D_{\mu, 0}^j(\phi_\pi, \theta_\pi, 0) \frac{1}{2} \frac{1 + (-1)^j}{2} \\
 &\langle J_\gamma - \lambda_\gamma; j\mu | J\mu - \lambda_\gamma \rangle \frac{1}{\sqrt{2}} [\delta_{\lambda_\gamma, 1} + \delta_{\lambda_\gamma, -1} P(-1)^{J_\gamma - 1}] V_{j, J_\gamma}(s)
 \end{aligned}
 \tag{A1}$$

1021 where the parity, total angular momentum, and helicity  
 1022 of the pair of pseudoscalars are given by  $P$ ,  $j$ , and  $\mu$ ,  
 1023 respectively. The  $D$  functions are the familiar Wigner  
 1024 D-matrix elements. The angular momentum of the pho-  
 1025 ton,  $J_\gamma$ , is related to the nuclear radiative (E1, M2, E3,  
 1026 etc.) transitions. Each amplitude is characterized by the  
 1027 angular momentum of the photon and the angular mo-  
 1028 mentum of the pseudoscalar pair. The possible values of  
 1029  $J_\gamma$  are limited by the conservation of angular momentum.  
 1030 The helicity of the radiative photon is given by  $\lambda_\gamma$ . The  
 1031 total angular momentum and polarization of the  $J/\psi$  are  
 1032 given by  $J$  and  $M$ , respectively. Finally,  $N_j = \sqrt{\frac{2j+1}{4\pi}}$  is  
 1033 a normalization factor.

1034 The angles  $(\phi_\gamma, \theta_\gamma)$  are the azimuthal and polar angles  
 1035 of the photon in the rest frame of the  $J/\psi$ , where the  
 1036 direction of the  $J/\psi$  momentum defines the x-axis. The  
 1037 angles  $(\phi_\pi, \theta_\pi)$  are the azimuthal and polar angles of one  
 1038  $\pi^0$  in the rest frame of the  $\pi^0\pi^0$  pair, with the -z axis  
 1039 along the direction of the photon momentum and the x-  
 1040 axis is defined by the direction perpendicular to the plane  
 1041 shared by the beam and the z-axis.

1042 Parity is a conserved quantity for strong and elec-  
 1043 tromagnetic interactions. Hence, for  $J/\psi$  radiative de-  
 1044 cays,  $P = (-1)^j$  must be positive. This means that the  
 1045 only intermediate states available have  $j^P = 0^+, 2^+, 4^+$ ,  
 1046 etc. Additionally, isospin conservation in strong inter-  
 1047 actions requires  $I^G$  for the intermediate state to be  $0^+$   
 1048 (isoscalar). The complex function  $V_{j, J_\gamma}(s)$  describes the

1049  $\pi^0\pi^0$  production and decay dynamics. In order to min-  
 1050 imize the model dependence of the mass independent  
 1051 analysis, the dynamical amplitude is replaced by a (com-  
 1052 plex) free parameter in the unbinned extended maximum  
 1053 likelihood fit. Thus, the amplitude, in a region around  $s$   
 1054 is given by

$$U^{M,\lambda_\gamma}(\vec{x}, s) = \sum_{j, J_\gamma} V_{j, J_\gamma} A_{j, J_\gamma}^{M,\lambda_\gamma}(\vec{x}), \tag{A2}$$

1055 where

$$\begin{aligned}
 A_{j, J_\gamma}^{M,\lambda_\gamma}(\vec{x}) &= N_{J_\gamma} N_j D_{M, \mu - \lambda_\gamma}^J(\pi + \phi_\gamma, \pi - \theta_\gamma, 0) \\
 &D_{\mu, 0}^j(\phi_\pi, \theta_\pi, 0) \frac{1}{2} \frac{1 + (-1)^j}{2} \\
 &\langle J_\gamma - \lambda_\gamma; j\mu | J\mu - \lambda_\gamma \rangle \\
 &\frac{1}{\sqrt{2}} [\delta_{\lambda_\gamma, 1} + \delta_{\lambda_\gamma, -1} P(-1)^{J_\gamma - 1}],
 \end{aligned}
 \tag{A3}$$

1056 and  $\{j, J_\gamma\}$  represents the unique amplitudes accessible  
 1057 for the given set of observables,  $\{M, \lambda_\gamma\}$ .

## Appendix B: Ambiguities

1058 One of the challenges of amplitude analysis is the issue  
 1059 of ambiguous solutions, two solutions that give the same  
 1060 distribution (eg. Ref. [7]). In this section, the ambiguous  
 1061 solutions for radiative  $J/\psi$  decays to  $\pi^0\pi^0$  are studied.  
 1062

To determine the angular dependence of the amplitudes, it is necessary to write the decay amplitude  $A_{j,J_\gamma}^{M,\lambda_\gamma}(\vec{x})$ , which is given in Eq. (A1), explicitly as a function of the angles  $(\phi_\gamma, \theta_\gamma)$  and  $(\phi_\pi, \theta_\pi)$ . The Clebsch Gordan factors in the amplitude restrict the signs of  $\mu$  to be the same as that of  $\lambda_\gamma$ . Thus, for  $j = 2$  and  $\lambda_\gamma = 1$ , only the values  $\mu = 0, 1, 2$  give non-zero amplitude contributions. It is also important to note that the Clebsch Gordan coefficients will change sign under  $\lambda_\gamma \rightarrow -\lambda_\gamma$ , but only for  $J_\gamma = 2$ . This will cancel the delta functions in the decay amplitude with the result

$$A_{j,J_\gamma}^{M,\lambda_\gamma}(\vec{x}) = \sum_{\mu} c_{j,\mu}^{J_\gamma,\lambda_\gamma} N_{J_\gamma} N_j e^{-iM(\pi+\phi_\gamma)} d_{M,\mu-\lambda_\gamma}^1(\pi-\theta_\gamma) \times e^{-i\mu\phi_\pi} d_{\mu,0}^j(\theta_\pi) \frac{1}{\sqrt{2}} [\delta_{\lambda_\gamma,1} + \delta_{\lambda_\gamma,-1} (-1)^{J_\gamma-1}] \quad (\text{B1})$$

where the constants  $c_{j,\mu}^{J_\gamma,\lambda_\gamma}$  contain the Clebsch-Gordan coefficients.

Recall that, for the Wigner small  $d$ -matrix elements,  $d_{1,\pm 1}^1(\pi-\theta) = d_{1,\mp 1}^1(\theta)$  and  $d_{1,0}^1(\pi-\theta) = d_{1,0}^1(\theta)$ . Then,  $d_{M,\mu-\lambda_\gamma}^1(\pi-\theta) = d_{M,\lambda_\gamma-\mu}^1(\theta)$ . Also, note that the restrictions on  $\mu$  mean that the quantity  $\mu - \lambda_\gamma = \pm 1, 0$ . It is also useful to note that  $\mu - \lambda_\gamma = \lambda_\gamma, 0, -\lambda_\gamma$ , for  $\mu = \pm 2, \pm 1, 0$  respectively. The usefulness of these features appears when one writes out the intensity for a given choice of  $M$  and  $\lambda_\gamma$ . It is also useful to plug in the values for the constants, which are given in Table III. The intensity in bin  $\alpha$  for a given choice of observables is then given by

$$I_\alpha(\vec{x}) = \sum_{M,\lambda_\gamma} |h_0(\theta_\pi) d_{M,\lambda_\gamma}^1(\theta_\gamma) e^{i\lambda_\gamma\phi_\pi} + h_1(\theta_\pi) d_{M,0}^1(\theta_\gamma) + h_2(\theta_\pi) d_{M,-\lambda_\gamma}^1(\theta_\gamma) e^{-i\lambda_\gamma\phi_\pi}|^2. \quad (\text{B2})$$

where terms with the same angular dependencies have been grouped according to

$$\begin{aligned} h_0(\theta_\pi) &= \sqrt{3}V_{0,1} + \sqrt{\frac{3}{2}}(V_{2,1} + \sqrt{5}V_{2,2} + 2V_{2,3})d_{0,0}^2(\theta_\pi) \\ h_1(\theta_\pi) &= \frac{1}{\sqrt{2}}(3V_{2,1} + \sqrt{5}V_{2,2} - 4V_{2,3})d_{1,0}^2(\theta_\pi) \\ h_2(\theta_\pi) &= (3V_{2,1} - \sqrt{5}V_{2,2} + V_{2,3})d_{2,0}^2(\theta_\pi) \end{aligned} \quad (\text{B3})$$

and the subscripts on the production amplitudes represent the possible combinations of  $j$  and  $J_\gamma$ . The following calculations apply for each bin individually.

TABLE III. The constant factors in Eq. (B1) are given here.

$$\begin{aligned} c_{0,0}^{J_\gamma,\lambda_\gamma} &= 1 \\ c_{2,0}^{1,\pm 1} &= \sqrt{\frac{1}{10}} \quad c_{2,0}^{2,\pm 1} = \pm \sqrt{\frac{3}{10}} \quad c_{2,0}^{3,\pm 1} = \sqrt{\frac{6}{35}} \\ c_{2,1}^{1,\pm 1} &= \sqrt{\frac{3}{10}} \quad c_{2,1}^{2,\pm 1} = \pm \sqrt{\frac{1}{10}} \quad c_{2,1}^{3,\pm 1} = -\sqrt{\frac{8}{35}} \\ c_{2,2}^{1,\pm 1} &= \sqrt{\frac{3}{5}} \quad c_{2,2}^{2,\pm 1} = \mp \sqrt{\frac{1}{5}} \quad c_{2,2}^{3,\pm 1} = \sqrt{\frac{1}{35}} \end{aligned}$$

The amplitudes for which  $M$  and  $\lambda_\gamma$  have the same (opposite) sign,  $M = \lambda_\gamma = \pm 1$  ( $M = -\lambda_\gamma = \pm 1$ ) are

related to each other by a sign change in the exponential factor. Note that the terms with a factor of  $d_{M,0}^1$  will change sign under  $M \rightarrow -M$  and terms with a factor of  $d_{\mu,0}^j$  will change sign under  $\lambda_\gamma \rightarrow -\lambda_\gamma$ . Then, the intensity becomes

$$\begin{aligned} I(\vec{x}) &= \sum_{M=\lambda_\gamma=\pm 1} |h_0(\theta_\pi) d_{1,1}^1(\theta_\gamma) e^{\pm i\phi_\pi} + h_1(\theta_\pi) d_{1,0}^1(\theta_\gamma) \\ &\quad + h_2(\theta_\pi) d_{1,-1}^1(\theta_\gamma) e^{\mp i\phi_\pi}|^2 \\ &+ \sum_{M=-\lambda_\gamma=\pm 1} |h_0(\theta_\pi) d_{1,-1}^1(\theta_\gamma) e^{\pm i\phi_\pi} - h_1(\theta_\pi) d_{1,0}^1(\theta_\gamma) \\ &\quad + h_2(\theta_\pi) d_{1,1}^1(\theta_\gamma) e^{\mp i\phi_\pi}|^2. \end{aligned} \quad (\text{B4})$$

Note that the term with  $h_1(\theta_\pi)$  has changed sign in the opposite combination. The properties of small  $d$  functions,  $d_{m',m}^j(\theta) = (-1)^{m-m'} d_{m,m'}^j(\theta) = d_{-m,-m'}^j(\theta)$ , have been used to write the incoherent pieces of the intensity in the same way.

It is instructive to write the intensity function as

$$\begin{aligned} I(\vec{x}) &= f_0 + f_1 \cos 2\theta_\gamma + \frac{1}{2} f_2 \cos 2\phi_\pi \\ &\quad + \frac{1}{2} f_3 \sin 2\theta_\gamma \cos \phi_\pi - \frac{1}{2} f_4 \cos 2\theta_\gamma \cos 2\phi_\pi, \end{aligned} \quad (\text{B5})$$

where

$$\begin{aligned} f_0 &= \frac{3}{2} [(h_0)^2 + (h_2)^2] + (h_1)^2 \\ f_1 &= \frac{1}{2} [(h_0)^2 + (h_2)^2] - (h_1)^2 \\ f_2 &= f_4 = (h_0 h_2^* + h_0^* h_2) \\ f_3 &= \sqrt{2} (-h_0 h_1^* - h_0^* h_1 + h_2 h_1^* + h_2^* h_1). \end{aligned} \quad (\text{B6})$$

Now, if a set of amplitude couplings,  $V$ , have been determined by fitting the intensity function in Eq. (B5) to the data, ambiguities would arise if an alternative set of couplings,  $V'$ , would give the same angular dependence as the original set. In other words, the new set of amplitudes must give the same values for the  $f_i$  functions ( $f'_i = f_i$ ). Consider  $f_2$ , which can be written as a linear combination of two quadratic forms

$$f_2 = \frac{1}{2} (|h_0 + h_2|^2 - |h_0 - h_2|^2). \quad (\text{B7})$$

1114 These quadratic forms are given by

$$|h_0 \pm h_2|^2 = [\cos^2 \theta_\pi (3a_1 \mp a_3) + (b - a_1 \pm a_3)] \times [\cos^2 \theta_\pi (3a_1^* \mp a_3^*) + (b^* - a_1^* \pm a_3^*)], \quad (\text{B8})$$

1115 where for simplicity the production coefficients have been  
1116 combined into new variables given by

$$\begin{aligned} b &= \sqrt{3}V_{0,1} \\ a_1 &= \frac{\sqrt{6}}{4}(V_{2,1} + \sqrt{5}V_{2,2} + 2V_{2,3}) \\ a_2 &= -\frac{\sqrt{3}}{4}(3V_{2,1} + \sqrt{5}V_{2,2} - 4V_{2,3}) \\ a_3 &= \frac{\sqrt{6}}{4}(3V_{2,1} - \sqrt{5}V_{2,2} + V_{2,3}). \end{aligned} \quad (\text{B9})$$

1117 Since only the absolute square of each combination of  
1118  $h_0$  and  $h_2$  appears in the intensity, nontrivial ambiguous  
1119 solutions only appear when the production coefficients  
1120 are replaced by their complex conjugate for one choice  
1121 of sign in Eq. (B8). That is, if  $u_1 = (b, a_1, a_2, a_3)$  and  
1122  $u_2 = (b', a'_1, a'_2, a'_3)$ , the solutions  $\{u_1, u_2\}$  and  $\{u_1, u_2^*\}$   
1123 should give consistent values for  $h_0 \pm h_2$ . This requires  
1124 that either

$$\begin{aligned} h'_0 + h'_2 &= h_0^* + h_2^* \\ h'_0 - h'_2 &= h_0 - h_2 \end{aligned} \quad (\text{B10})$$

1125 OR

$$\begin{aligned} h'_0 + h'_2 &= h_0 + h_2 \\ h'_0 - h'_2 &= h_0^* - h_2^* \end{aligned} \quad (\text{B11})$$

1126 Therefore, either

$$\begin{aligned} 3a'_1 - a'_3 &= 3a_1^* - a_3^* \\ b' - a'_1 + a'_3 &= b^* - a_1^* + a_3^* \\ 3a'_1 + a'_3 &= 3a_1 + a_3 \\ b' - a'_1 - a'_3 &= b - a_1 - a_3 \end{aligned} \quad (\text{B12})$$

1127 OR

$$\begin{aligned} 3a'_1 - a'_3 &= 3a_1 - a_3 \\ b' - a'_1 + a'_3 &= b - a_1 + a_3 \\ 3a'_1 + a'_3 &= 3a_1^* + a_3^* \\ b' - a'_1 - a'_3 &= b^* - a_1^* - a_3^*. \end{aligned} \quad (\text{B13})$$

1128 Both Eq. (B12) and Eq. (B13) require that

$$\text{Im } b = -2 \text{Im } a_1. \quad (\text{B14})$$

1129 The difference between Eq. (B12) and Eq. (B13) is a sign  
1130 change for imaginary part of each amplitude. This differ-  
1131 ence is equivalent to the trivial ambiguities discussed in  
1132 section IV D. Let us choose the phase convention given  
1133 by Eq. (B12). Finally, invariance of  $f_1$ , given the condi-  
1134 tions above, requires that  $a'_2 = a_2$ .

1135 Using the conditions in Eq. (B12) and the constraint  
1136  $a'_2 = a_2$ , the alternate set of solutions can be written in  
1137 terms of the original set as

$$\begin{aligned} \text{Re } V'_{0,1} &= \text{Re } V_{0,1} \\ \text{Im } V'_{0,1} &= -\frac{1}{3\sqrt{2}}(3 \text{Im } V_{2,1} - \sqrt{5} \text{Im } V_{2,2} + \text{Im } V_{2,3}) \\ \text{Re } V'_{2,1} &= \text{Re } V_{2,1} \\ \text{Im } V'_{2,1} &= \text{Im } V_{2,1} + \frac{2\sqrt{5}}{3} \text{Im } V_{2,2} + \frac{5}{6} \text{Im } V_{2,3} \\ \text{Re } V'_{2,2} &= \text{Re } V_{2,2} \\ \text{Im } V'_{2,2} &= -\text{Im } V_{2,2} - \frac{\sqrt{5}}{2} \text{Im } V_{2,3} \\ \text{Re } V'_{2,3} &= \text{Re } V_{2,3} \\ \text{Im } V'_{2,3} &= \text{Im } V_{2,3}. \end{aligned} \quad (\text{B15})$$

1138 Note that the last two lines of Eq. (B15) indicate that  
1139 the ambiguous solution for the  $2^{++}$  E3 amplitude is re-  
1140 dundant with the original solution. That is, the  $2^{++}$  E3  
1141 amplitude does not exhibit multiple solutions.

1142 In a practical sense, these results are useful to compare  
1143 the mathematical predictions to what is found experi-  
1144 mentally. Essentially, the predicted ambiguous partner  
1145 for a set of fit results in a given bin may be calculated in  
1146 the following way. First, the results must be rotated in  
1147 phase space such that the condition in Eq. (B14) is sat-  
1148 isfied. Next, the ambiguous partner may be determined  
1149 using Eq. (B15). Finally, this predicted solution must be  
1150 rotated back into the original phase convention. Now, the  
1151 predicted ambiguous partner may be compared with the  
1152 experimentally determined fit results. Studies show that  
1153 the mathematically predicted ambiguities match those  
1154 found experimentally.

### 1155 Appendix C: Supplemental Materials

1156 In addition to the figures presented here, the results  
1157 of the mass independent analysis in each bin of  $M_{\pi^0\pi^0}$   
1158 are included in the supplemental materials [37]. This  
1159 includes the intensities of each amplitude and the three  
1160 phase differences for each bin of  $M_{\pi^0\pi^0}$ . The two ambigu-  
1161 ous solutions of the nominal results are separated into  
1162 two text files, while one additional text file contains the  
1163 alternate results in the region where they are not redun-  
1164 dant with the nominal results. Note that these results  
1165 contain only statistical errors.

1166 It is important to reiterate that errors reported in the  
1167 supplemental results (and in the figures in the text) are  
1168 derived from the covariance matrix of the fit parameters.  
1169 That is, they are valid in the Gaussian limit, a limit that  
1170 cannot be guaranteed for all parameters in the analy-  
1171 sis. Therefore the use of these results in a subsequent fit  
1172 to parameters of interest cannot be expected to produce  
1173 statistically rigorous values of the parameters. Likewise

1174 a  $\chi^2$  or likelihood-ratio test of a model describing the 1194 sis, in which the Breit-Wigner model is directly fit to the  
 1175 results cannot be rigorously constructed. 1195 same mock data, the parameter errors in the model fit to  
 1176 An attempt to quantify the potential systematic bias 1196 the MI results were generally larger, typically within a  
 1177 in subsequent analyses was made as follows. First, a sam- 1197 factor of two, but in some cases by up to a factor of ten.  
 1178 ple of MC with equivalent statistical precision to the data 1198 To probe the scale of the systematic deviations of the  
 1179 was generated using a model consisting of a coherent sum 1199 fitted values from the true input values used to gener-  
 1180 of Breit-Wigner resonances in a way that best approxi- 1200 ate our MC sample, for each amplitude we used the true  
 1181 mates the data. A mass independent amplitude analysis 1201 value of the coupling instead of the fitted value and com-  
 1182 was performed on this MC sample using the same proce- 1202 puted (1) the total intensity integrated over all phase  
 1183 dure that was applied to the actual data reported in 1203 space and (2) the fit fraction (ratio of individual ampli-  
 1184 this analysis. The results of this mass independent anal- 1204 tude intensity to total intensity). We observe the de-  
 1185 ysis of the MC sample were then fit with a Breit-Wigner 1205 viations in (1) to be at or below the 1% level for all  
 1186 model, the same model with which they were generated, 1206 amplitudes and deviations in (2) to be at or below 2%  
 1187 where the couplings of the Breit-Wigner distributions in 1207 on an absolute scale for all amplitudes. For small am-  
 1188 the model were allowed to float as free parameters. While 1208 plitudes, this means that relative deviations in intensity  
 1189 most fit parameters exhibited typical Gaussian fluctua- 1209 may occur at a level of 10-90%. This suggests validity  
 1190 tions about their known input values, there were some 1210 and precision at a level sufficient for model development;  
 1191 non-Gaussian outliers. About one-third of the parame- 1211 however, rigorous values for any model parameters can  
 1192 ters exhibited deviations from input at or above the three 1212 only be reliably obtained by fitting the given model di-  
 1193 sigma level. In comparison with a mass dependent analy- 1213 rectly to the data.

- 
- 1214 [1] J. Beringer *et al.* [Particle Data Group], Phys. Rev. D 1252  
 1215 **86**, 010001 (2012). 1253  
 1216 [2] G. S. Bali, K. Shilling, A. Hulsebos, A. C. Irving, 1254  
 1217 C. Michael, and P. Stephenson, Phys. Lett. B **309**, 378 1255  
 1218 (1993). 1256  
 1219 [3] C. J. Morningstar and M. J. Peardon, Phys. Rev. D **60**, 1257  
 1220 034509 (1999). 1258  
 1221 [4] Y. Chen, A. Alexandru, S. J. Dong, T. Draper, I. Hor- 1259  
 1222 vath, F. X. Lee, K. F. Liu, N. Mathur, C. Morn- 1260  
 1223 ingstar, M. Peardon, S. Tamhankar, B. L. Young, and 1261  
 1224 J. B. Zhang, Phys. Rev. D **73**, 014516 (2006). 1262  
 1225 [5] W. Ochs, J. Phys. G **40**, 043001 (2013). 1263  
 1226 [6] J. R. Pelaez and F. J. Yndurain, Phys. Rev. D **71**, 074016 1264  
 1227 (2005). 1265  
 1228 [7] J. Gunter *et al.* [E852 Collaboration], Phys. Rev. D **64**, 1266  
 1229 072003 (2001). 1267  
 1230 [8] A. Abele *et al.* [Crystal Barrel Collaboration], Phys. Lett. 1268  
 1231 B **380**, 453 (1996). 1269  
 1232 [9] R. Bellazzini *et al.* [GAMS Collaboration], Phys. Lett. B 1270  
 1233 **467**, 296 (1999). 1271  
 1234 [10] M. Ablikim *et al.* [BES Collaboration], Phys. Lett. B **645**, 1272  
 1235 19 (2007). 1273  
 1236 [11] M. Ablikim *et al.* [BES Collaboration], Phys. Lett. B **607**, 1274  
 1237 243 (2005). 1275  
 1238 [12] M. Ablikim *et al.* [BES Collaboration], Phys. Lett. B **598**, 1276  
 1239 149 (2004). 1277  
 1240 [13] M. Ablikim *et al.* [BES Collaboration], Phys. Lett. B **603**, 1278  
 1241 138 (2004). 1279  
 1242 [14] J. P. Lees *et al.* [BaBar Collaboration], Phys. Rev. D **85**, 1280  
 1243 112010 (2012). 1281  
 1244 [15] G. Bonvicini *et al.* [CLEO Collaboration], Phys. Rev. D 1282  
 1245 **76**, 012001 (2007). 1283  
 1246 [16] J. R. Batley *et al.* [NA48/2 Collaboration], Eur. Phys. J. 1284  
 1247 C **54**, 411 (2008). 1285  
 1248 [17] T. Mori *et al.* [Belle Collaboration], Phys. Rev. D **75**, 1286  
 1249 051101 (2007). 1287  
 1250 [18] A. Aloisio *et al.* [KLOE Collaboration], Phys. Lett. B 1288  
 1251 **537**, 21 (2002). 1289  
 1252 [19] V. Anisovich and A. Sarantsev, Eur. Phys. J. A **16**, 229  
 1253 (2003).  
 1254 [20] M. Ablikim *et al.* [BES Collaboration], Phys. Lett. B **642**,  
 1255 441 (2006).  
 1256 [21] R. M. Baltrusaitis *et al.* [Mark-III Collaboration], Phys.  
 1257 Rev. D **35**, 2077 (1987).  
 1258 [22] J.E. Augustin *et al.* [DM2 Collaboration], Z. Phys. C **36**,  
 1259 369 (1987).  
 1260 [23] J. Z. Bai *et al.* [BES Collaboration], Phys. Rev. Lett. **76**,  
 1261 3502 (1996).  
 1262 [24] L. Kopke and N. Wermes, Phys. Rep. **36**, 67 (1989).  
 1263 [25] J. Z. Bai *et al.* [BES Collaboration], Phys. Rev. Lett. **81**,  
 1264 3091 (1998).  
 1265 [26] M. Ablikim *et al.* [BES Collaboration], Chin. Phys. C **36**,  
 1266 915 (2012).  
 1267 [27] M. Ablikim *et al.* [BES Collaboration], The total number  
 1268 of  $J/\psi$  events taken in 2009 and 2012 is determined to  
 1269 be  $1310.6 \times 10^6$  with an uncertainty 0.8% with the same  
 1270 approach as that used in Ref. [26]. (2014).  
 1271 [28] M. Ablikim *et al.* [BES Collaboration], Nucl. Instr. and  
 1272 Metho. A **614**, 345 (2010).  
 1273 [29] Z. Y. Deng, G. F. Cao, C. D. Fu, M. He, H. M. Liu, Y. J.  
 1274 Mao, Y. Xia, Z. Y. You, Y. Yuan, and R. Tang, Chinese  
 1275 Physics C **30**, 371 (2006).  
 1276 [30] S. Jadach, B. F. L. Ward, and Z. Was, Comput. Phys.  
 1277 Commun. **130**, 260 (2000).  
 1278 [31] D. J. Lange, Nucl. Instrum. Meth. A **462**, 152 (2001).  
 1279 [32] J. C. Chen, G. S. Huang, X. R. Qi, D. H. Zhang, and  
 1280 Y. S. Zhu, Phys. Rev. D **62**, 034003 (2000).  
 1281 [33] T. Kunihiro, Prog. Theor. Phys. Supplement **149**, 56  
 1282 (2003).  
 1283 [34] C. Amsler and N. A. Tornqvist, Phys. Rep. **389**, 61  
 1284 (2004).  
 1285 [35] F. E. Close and A. Kirk, Eur. Phys. J. C **21**, 531 (2001).  
 1286 [36] L. S. Celenza, S. F. Gao, B. Huang, H. Wang, and C. M.  
 1287 Shakin, Phys. Rev. C **61**, 035201 (2000).  
 1288 [37] See supplemental material at [url will be inserted by pub-  
 1289 lisher] for text files that contain the intensities of each

<sup>1290</sup> amplitude and the three phase differences for each bin of <sup>1291</sup> the mass independent amplitude analysis.